Acta metall. Vol. 37, No. 7, pp. 1693–1715, 1989
Printed in Great Britain.

0001-6160/89 $3.00 + 0.00

OVERVIEW NO. 83

A TIGHT-BINDING STUDY OF GRAIN BOUNDARIES IN SILICON

A. T. PAXTON† and A. P. SUTTON

Department of Metallurgy and Science of Materials, Oxford University, Parks Road, Oxford OX1 3PH, England

(*Received* 19 *August* 1988)

Abstract—A simple empirical tight-binding model for silicon is propounded and used to compute the atomic and electronic structures of three symmetrical tilt grain boundaries and the intrinsic stacking fault. The ability of the model to describe silicon in a variety of crystal structures is tested and it is shown to be satisfactory for simulating defects in the diamond structure. The effect of charge transfer on the energy and stability of the grain boundaries is assessed. Interatomic forces and energies are computed in real space using a rotationally invariant formulation of the recursion method. Five proposed reconstructions of the $(11\bar{2})$ symmetrical tilt boundary are studied in detail and good agreement is achieved with results from electron microscopy and diffraction. The $(1\bar{3}0)$ and (111) symmetrical tilt boundaries have also been modelled successfully. Comparison is made between the computed electronic structures of the boundaries, reported in this work and by other authors, and experimental measurements of the densities of states at grain boundaries. The existence of band tails and midgap continua in the experimental measurements and the absence of both of these features in the models are two notable points of disagreement. Some fundamental questions about localisation of electronic states at grain boundaries are raised.

Résumé—Nous proposons un modèle empirique simple de liaisons fortes dans le silicium et nous l'utilisons pour simuler les structures electronique et atomique de trois joints de grains de flexion et de la faute d'empilement intrinsèque. On teste la capacité du modèle à décrire le silicium en diverses structures cristallines et on montre qu'il est satisfaisant pour décrire les défauts dans la structure diamant. L'effet du transfert de charge sur l'énergie et la stabilité des joints de grains est évalué. Les forces interatomiques et les énergies sont simulées dans l'espace réel en utilisant une formulation rationnelle invariante de la méthode de récurrence. On étudie cinq reconstructions proposées pour le joint de flexion symétrique $(11\bar{2})$ et on arrive à un bon accord avec les résultats de microscopie et de diffraction electroniques. Les joints de flexion symétriques $(1\bar{3}0)$ et (111) ont aussi été modélisés avec succés. On établit une comparaison entre les structures électroniques simulées des joints présentées dans ce travail ou proposées par d'autres auteurs, et les mesures expérimentales de densité d'états aux joints de grains. L'existence de queues de bande et d'un continuum dans la discontinuité d'énergie que l'on trouve dans les mesures expérimentales et que l'on ne trouve pas dans les modèles, sont deux points notables de désaccord. Quelques questions fondamentales sur la localisation d'états electroniques dans les joints de grains sont soulevées.

Zusammenfassung—Für Silizium wird ein einfaches tight-binding-Modell vorgeschlagen. Damit werden die atomaren und die elektronischen Strukturen von drei symmetrischen Kippkorngrenzen und des intrinsischen Stapelfehlers berechnet. Die Fähigkeit des Modells, Silizium in einer Reihe von verschiedenen Strukturen zu beschreiben, wird geprüft: das Modell ist geeignet, Defekte in der Diamantstruktur zufriedenstellend zu beschreiben. Der Einfluß der Ladungsverschiebung auf Energie und Stabilität von Korngrenzen wird geprüft. Interatomare Kräfte und Energien werden im Ortsraum mit einer gegen Rotationen invarianten Formulierung der Rekursionsmethode berechnet. Ausführlich werden fünf verschiedene Rekonstruktionen der symmetrischen $(11\bar{2})$-Kippkorngrenze untersucht; die Ergebnisse stimmen gut mit entsprechenden elektronenmikroskopischen Untersuchungen überein. Die symmetrischen $(1\bar{3}0)$- und (111)-Kippkorngrenzen werden außerdem erfolgreich behandelt. Die in dieser Arbeit berechneten elektronischen Strukturen der Korngrenzen und theoretische Ergebnisse anderer Autoren werden mit experimentellen Messungen der Zustandsdichte an Korngrenzen verglichen. Zwei wichtige Widersprüche zwischen Experiment und Theorie sind zu bemerken: im Experiment finden sich auslaufende Bänder und Kontinua der Zustände in der Bandmitte, beides fehlt in den Computererergebnissen. Es werden einige grundlegende Fragen zu der Lokalisierung elektronischer Zustände an Korngrenzen aufgeworfen.

1. INTRODUCTION

In semiconductors high resolution transmission electron microscopy and measurements of the local densities of electronic states at grain boundaries by a variety of techniques have revealed much more detailed information about the atomic and electronic structures of grain boundaries than has been achieved by modelling [see 1–5 for reviews]. Indeed much of the information obtained from experiment about the

†Present address: Max-Planck-Institut für Festkörperforschung, D-7000 Stuttgart 80; Heisenbergstrasse 1, F.R.G.

atomic and electronic structures of grain boundaries has yet to be satisfactorily modelled. In this paper we present a study of grain boundaries in pure silicon which addresses some of the results on structure and electronic properties found by experiment. Because the model we use has its basis in quantum mechanics we believe it to be appropriate for tackling the interdependence of the atomic and electronic structures of grain boundaries. At the same time the model is physically transparent and susceptible to a range of simplifying approximations, most of which can be removed if desired. Brief reports of this work have already been published [6, 7]. A detailed account of the theory underlying the model has appeared in [8].

In contrast to grain boundaries in metals there has been relatively little modelling of the atomic structures of grain boundaries in semiconductors. In most instances valence force fields [e.g. 9–12], or classical interatomic potentials [e.g. 13] have been used or geometrical models have been constructed [14, 15]. Obviously no insight into the electronic structure of the boundaries is gained from these models. More seriously, there is no account taken in these models of the change in bonding at the boundary and how that influences the boundary structure and energy. This has provoked several authors to turn to a description of interatomic forces in semiconductors that is quantum mechanically based. Perhaps the simplest model is Harrison's bond orbital approximation [16] which has been applied by Kohyama *et al.* [17] to symmetrical [110] tilt boundaries and (111) twist boundaries in Si. In essence this method is not very different from a valence force field since no rehybridisation is allowed and little information about the electronic structure of the boundary is gained. Thomson and Chadi [18] carried out the first tight-binding study of a grain boundary in Si. They applied the method which was pioneered by Chadi in his studies of surfaces of Si [19] to the (221) symmetrical tilt boundary. This method is very similar to our own. The principal differences are (i) we solve the tight-binding Hamiltonian in real space using the recursion method [20] whereas in Chadi's approach it is solved in **k** space by matrix diagonalization, (ii) we require local charge neutrality as a form of self-consistency whereas in Chadi's approach there is no attempt at self-consistency, (iii) the pair potentials are different. In two recent papers Kohyama *et al.* [21] have used Chadi's method to study the $(1\bar{3}0)$ and $(11\bar{2})$ symmetrical tilt boundaries in Si, since detailed information about these boundaries has been obtained by electron microscopy [22]. For the same reason, but independently of Kohyama *et al.*, we studied these boundaries with our method and published a brief report in [7]. DiVincenzo *et al.* [23] compared the results obtained using Chadi's method with those from an *ab initio* local density functional calculation applied to two reconstructions of the (221) symmetrical tilt boundary in Si. The relative boundary energies for the two reconstructions compared well in the two methods. More significantly two tests were made, using the *ab initio* program, to check the stability of the boundary structure, which was obtained by Chadi's method. It was found [23] that atom positions agreed to within 0.05Å and the bicrystal phonon frequencies agreed extremely well. The most ambitious *ab initio* determinations of a grain boundary structure was performed by Payne *et al.* [24] using a modified form [25] of the method of Car and Parrinello [26]. Payne *et al.* considered the structure of the $\Sigma = 5$ (001) twist boundary in Ge. In principle the Car–Parrinello method should be the most accurate of all presently available since it is capable of treating dynamically approximately 100 atoms in Ge and all their valence electrons (with present computing power). Payne *et al.* [24] were not so ambitious and did not attempt to simulate true ionic dynamics; instead they performed a simultaneous optimization of the electronic and ionic degrees of freedom by quenching the real kinetic energies of the ions and fictitious kinetic energies of the electrons into the nearest local minimum. Thus the configuration space of the boundary was sampled rather like it is in a static simulation by selecting several starting configurations and *quenching* into the nearest metastable state. Like most *ab initio* methods using a plane wave basis set physical transparency is to some extent sacrificed for accuracy, and this has its drawbacks, although the work of Payne *et al.* is a remarkable achievement.

The rest of the paper is organized as follows. In Section 2 we describe the tight-binding approximation and quantities of physical and chemical interest such as the density matrix, the cohesive energy and interatomic forces. We believe that, at the present time, this is the only explicitly quantum-mechanical method capable of calculating inter-atomic forces, cohesive energies and electronic structure sufficiently rapidly for the relaxation of crystal defects having several hundreds of non-equivalent atoms. Our implementation of the recursion method is described in Section 3, where we have also made some comparisons with the **k**-space method of Chadi. Tests to ensure that the model guarantees that the diamond cubic structure is the lowest energy structure of Si are described in Section 4, together with a study of the intrinsic stacking fault and the (111) twin. The method we have used to relax grain boundaries is described in Section 5. Sections 6 and 7 contain the results of our studies of the $(11\bar{2})$ and $(1\bar{3}0)$ symmetrical tilt boundaries, and review what is known about these boundaries from electron microscopy experiments. The discussion in Section 8 is focussed on the model we have used, its solution, a comparison between the theoretical results for the electronic structure of grain boundaries and experimental measures, and finally a discussion of charge transfer and the importance of self-consistency in the model.

2. FUNDAMENTALS

2.1. The tight-binding approximation

Inter-atomic forces, cohesive energies and electronic structure are calculated within the semi-empirical tight-binding approximation. The method has its roots in the development of quantum chemistry in the 1930's [27] and was formulated for the solid state in a pioneering paper by Slater and Koster in 1954 [28]. The wavefunctions of the valence electrons are expressed as linear combinations of atomic-like orbitals (LCAO). The method is semi-empirical because rather than evaluating the integrals involving products of two orbitals and an atom-centred potential, these integrals, which are matrix elements of the Hamiltonian operator, $\hat{H}$, are regarded as disposable parameters which are empirically fitted to the energy bands of the crystal in question. Recently, an extremely simple formulation of the method was devised for semiconductors by Harrison [16, 29], which involves only four such disposable parameters which he calls $V_{ss\sigma}$, $V_{sp\sigma}$, $V_{pp\sigma}$ and $V_{pp\pi}$. These are fundamental bond (or *hopping* or *transfer* or *resonance*) integrals between the s and p orbitals on neighbouring atoms which comprise the minimal basis set in which the valence wavefunctions are to be expanded. The first two subscripts indicate the orbital type on the neighbouring atoms and the second gives the angular momentum character of the bond which results from the overlap of the two orbitals (that is, $a\ \sigma$ or π bond [27]). A fifth disposable parameter is the energy differences or *s–p splitting* $(\epsilon_p - \epsilon_s)$ between the p and s orbitals†. Explicit assumptions in Harrison's formulation are the vanishing of bond integrals between second and further neighbours in the tetrahedral lattice as well as integrals involving more than two atomic sites (the two-centre approximation), and orthogonality of the s and p orbitals on different atomic sites in the solid. Harrison's prescription makes it extremely easy to construct a Hamiltonian matrix (and thereby solve Schrödinger's equation) for any assembly of Si atoms, using the four bond integrals multiplied by geometric factors which account for the direction of the bond in relation to the cartesian axes to which the three p-orbitals are referred. These geometric factors result from the fundamental transformation properties under rotations of the spherical harmonic functions which enter the atomic orbitals, and are tabulated by Slater and Koster [28]. Thus the *angular dependence* of bond energy (and hence inter-atomic force) results from the non-spherically symmetric probability amplitude of the atomic orbitals with angular momentum, l, greater than zero (in this case the three perpendicular p-orbitals). The *radial dependence* of the inter-atomic force comes from a further proposal by Harrison, namely that the bond integrals decay in magnitude with the inverse square of the bond length. The argument behind this "$1/d^2$" scaling law is that it mimics the free-electron-like nature of the valence electrons in semiconductors as well as the known volume dependence of the bandwidth. For a pedagogical treatment of the method we refer the reader to Harrison's book [16].

2.2. The density matrix

Schrödinger's equation is solved by finding the eigenvalues and eigenvectors of the Hamiltonian matrix. These describe the allowed quantum states of the valence and conduction electrons in the assembly of atoms used to construct the Hamiltonian. The eigenvectors are columns of expansion coefficients of the wavefunctions expressed in the LCAO; the corresponding eigenvalues are the energies of these states. Suppose we have an assembly of N atoms‡, and on each atom we suppose there to be one s and three p orbitals. We label the atoms with indices $i, j \ldots$ and the orbitals with indices $\alpha, \beta \ldots$ so that the basis functions of the LCAO could be denoted $u_{i\alpha}$, $u_{j\beta}$ etc. The solutions of Schrödinger's equation, $\hat{H}\Psi_n = E_n\Psi_n$, in the tight-binding approximation appear in the following form:

$$\Psi_n = \sum_{i\alpha} c_n^{i\alpha} u_{i\alpha}. \tag{2.1}$$

$c_n^{i\alpha}$ are components of the eigenvector corresponding to the nth solution of Schrödinger's equation. The eigenenergy of this state will be denoted E_n and if the system contains $2n$ spin-degenerate electrons, the lowest n eigenstates will be occupied at zero temperatures. Only occupied states contribute to ground state properties, and we now define quantities of central importance in all that follows. These are matrix elements of the density operator [30–32] between an α-orbital on atom i and a β-orbital on atom j

$$\rho^{i\alpha, j\beta} = 2 \sum_{\substack{n \\ \text{(occupied)}}} c_n^{i\alpha} \bar{c}_n^{j\beta}. \tag{2.2}$$

A bar denotes complex conjugation; the summation is over the n lowest energy eigenstates and the factor 2 accounts for spin degeneracy. An extension to a non-orthogonal basis can be easily made [32], but for the present purpose and for simplicity of presentation we adhere to the usual assumption of an orthogonal basis (see above). All the information we need about the electronic structure of the atomic assembly is contained in the density matrix. Specifically, the diagonal element, $\rho^{i\alpha, i\alpha}$, is the number of electrons

†The parameters, in eV, actually used in our calculations are as follows [19d]: $V_{ss\sigma} = -1.9375$; $V_{sp\sigma} = 1.745$; $V_{pp\sigma} = 3.05$; $V_{pp\pi} = -1.075$; $(\epsilon_p - \epsilon_s) = 6.45$.

‡In the infinite crystal, N is infinite. To avoid infinite-dimensional matrices, each matrix element is usually multiplied by a wavevector-dependent Bloch phase factor which reduces the number of atoms explicitly entering the Hamiltonian to the number of atoms in the unit cell. This, of course, requires periodicity in three dimensions, which is not a property of defective solids. We will see later how Schrodinger's equation can be solved without recourse to Bloch's theorem.

occupying the α-orbital on atom i; while the off-diagonal element $\rho^{i\alpha,j\beta}$ is the partial order of the bond joining atoms i and j [27]. The total order of the bond (*bond order* for short) is this quantity summed over all the α and β types of orbital on atoms i and j. The bond order is half the difference between the number of bonding and antibonding states of the bond which are occupied. The reader is referred to an article by Pettifor [33] for a clear explanation and examples.

To recapitulate: we imagine an assembly of Si atoms in the solid state, for which we can construct a Hamiltonian matrix of simple bond integrals scaling with bond length like the inverse square, and multiplied by geometric factors determined by the bond angles. Only first neighbour bonds contribute. We determine density matrix elements from the Hamiltonian which then give us information on *orbital occupancies* (and hence the extent of any re-hybridisation between orbitals), and *bond orders* which measure the strength of each bond. To put this on a more quantitative basis and to discuss inter-atomic forces, we need to develop the method further.

2.3. *Cohesive energy and inter-atomic forces*

The density matrix has the useful property [30–32] that the expectation value of an operator, $\hat{O}$, is given by the trace of the matrix obtained by multiplying the density matrix by the matrix representation of $\hat{O}$. Thus, $\langle\hat{O}\rangle = \mathrm{Tr}[\hat{\rho}\hat{O}]$. Therefore the expectation value of the Hamiltonian, often called the band energy or "one-electron sum" is given in the LCAO representation by

$$E_{\text{band}} = \sum_{i\alpha j\beta} \rho^{i\alpha,j\beta} H_{j\beta,i\alpha}, \tag{2.3a}$$

$$= 2 \sum_{\substack{n \\ \text{(occupied)}}} E_n \tag{2.3b}$$

where $H_{i\alpha,j\beta}$ are matrix elements of the Hamiltonian described above. For two reasons, this quantity is not the total electronic energy of the solid [e.g. 34]:

1. Three contributions to the total energy remain.
   - (i) The electron–electron electrostatic energy (Hartree energy) has been counted twice in (2.3). So the Hartree energy must be subtracted from (2.3).
   - (ii) The many–body exchange-correlation energy is ignored in this one-electron picture and must be added in.
   - (iii) The electrostatic interaction between the positive ions must be added to get the total energy.

2. Schrödinger's equation should be solved iteratively to self-consistency. This means that the charge density obtained from the occupied eigenvectors should be consistent with the effective potential that went into constructing the Hamiltonian [35]. If Schrödinger's equation is not solved self-consistently the total electronic energy is not minimized.

The usual answer to the first problem in empirical tight-binding theory, is to write the total energy as a sum of two terms, the band energy plus a repulsive pairwise energy to model the remaining three terms [e.g. 19]. No satisfactory justification for treating these terms in the pair potential approximation has been given until recently. Harris [36] has noted that to calculate the total energy or binding energy reasonably accurately it is not necessary to solve the Schrödinger equation self-consistently. In density functional theory there is a variational principle according to which the total electronic energy of the system is a minimum at the self-consistent charge density distribution. Harris [36] exploited this principle by arguing that a first order error in the charge density gives rise to a second order (therefore smaller) error in the total electronic energy. Harris [36] and Sutton *et al.* [8] showed, using density functional theory, that the binding energy can be written in the form

$$E_{\text{B}} = E_{\text{cov}} + E_{\text{pro}} + E_{\text{rep}} \tag{2.4}$$

where E_{B} is the energy difference between the atoms in the solid and the same atoms infinitely separated *in vacuo*. The covalent bond energy, E_{cov}, is the sum of the covalent energies of all bonds in the solid, and it is equal to the band energy (2.3a) with the site diagonal terms removed

$$E_{\text{cov}} = \sum_{\substack{i\alpha j\beta \\ i\alpha \neq j\beta}} \rho^{i\alpha,j\beta} H_{j\beta,i\alpha} \tag{2.5}$$

E_{pro}, the promotion energy, is the energy change arising from differences in individual orbital occupation numbers between atoms infinitely separated and the same atoms condensed into the solid. E_{rep} is the repulsive energy representing the change in the total electrostatic (i.e. electron–electron, electron–ion and ion–ion) and exchange–correlation energies as the atoms at infinity are brought together to form the atomic assembly. In equation (2.4) the density matrix is not iterated to self-consistency and the Hamiltonian, which is expressed in terms of a superposition, ρ^{f}, of atomic density matrices, is solved once to produce an output density matrix ρ. Equation (2.4) is not exact but again the variational principle shows that the error involved is second order in the difference between ρ^{f} and the self-consistent density matrix. Sutton *et al.* [8] showed that to the same degree of approximation they were making for E_{cov} and E_{pro} the repulsive energy, E_{rep}, could be written as a sum of pair potentials. The variational principle indicates that errors involved in estimating analytic (as opposed to numerical) derivatives of the energy are larger. For example, the error in calculating analytically the force is of the same order as the difference between ρ and the self-consistent density matrix. For this reason to calculate forces analytically

it was argued [8] that at least an approximate form of self-consistency is required. The same authors [8] went on to develop an expression for the force, $\mathbf{F}^{ij}$, acting on atom i due to atom j in the atomic assembly. As an approximate self-consistency, a condition of *local charge neutrality* is imposed in which the orbital energies are adjusted to maintain neutral atoms. The interatomic force then may be written

$$\mathbf{F}^{ij} = -2\sum_{\alpha\beta} \rho^{i\alpha, j\beta} \nabla_i H_{j\beta, i\alpha} - \nabla_i E^{ij}_{\text{rep}}. \qquad (2.6)$$

Here ∇_i denotes differentiation with respect to the coordinates of atom i. This is trivial when applied to E^{ij}_{rep} which is the pair potential between atoms i and j. Differentiating the Hamiltonian matrix elements is also straight forward because of their simple radial and angular dependence. Satisfying the condition of local charge neutrality ensures that at least the diagonal elements of the Hamiltonian respond to the variations of potential as electronic charge is redistributed when atomic sites cease to be equivalent. If electrons attempt to accumulate on an atom, i, all its orbital energies, ϵ_α, are raised by an amount, Δ_i, just sufficient to raise their energy and restore local charge neutrality. The Δ's are determined self-consistently in an iterative algorithm [37, 38]. The expression for the binding energy given in equation (2.4), the approximation of E_{rep} by a sum of pair potentials, the approximation of self-consistency by local charge neutrality and the interatomic force given in equation (2.6) constitute the *tight-binding bond model* of [8]. Clearly it is not necessary to differentiate the band energy numerically as done, for example, by Legrand [39], which is a very time-consuming calculation since a small displacement of one atom will change the contribution to the energy from many other atoms in the assembly. The imposition of local charge neutrality has other advantages too:

1. Although it is achieved by varying on-site Hamiltonian matrix elements these diagonal terms do not contribute to the force of an atom. This is in contrast to other empirical tight-binding schemes [18, 19, 21] in which the on-site Hamiltonian matrix elements do not contribute to the force because they are not allowed to change at all.

2. It is a good approximation to self-consistency in semiconductors [37, 40] and an excellent one in metals, where perfect screening requires local charge neutrality [41].

3. There are no Madelung contributions to the total energy. This is in contrast to other empirical tight-binding schemes [18, 19, 21] where charge transfer is allowed to take place and the Madelung energy is simply ignored.

2.4. The pair potential

Finally, in this section, we make some remarks about the repulsive pair potential, which has also been discussed by van Schilfgaarde and Sher [42]. Although the repulsive energy is pairwise in the model of Sutton *et al.* [8], this assumes that the basis functions are actually atomic orbitals. Such a basis is non-orthogonal. In Si the significant non-orthogonality of the atomic orbitals will provide a large repulsive energy contribution to the covalent bond and promotion energies. Harrison [43] suggested that this contribution be added to the repulsive pair potential and, because it is so large, it must be understood to constitute the major part. Following Harrison [43], we therefore adopt a pair potential having inverse fourth power bond length dependence. This is motivated by the observation that the first order correction to the covalent bond and promotion energies due to the overlap scales as the product of the off-diagonal Hamiltonian and overlap matrix elements. The assumption here is that the off-diagonal Hamiltonian and overlap matrix elements both scale as $1/d^2$. However, as noted in [8], this correction is not strictly pairwise or environment independent. We discuss the pair potential further in Section 8.2.

3. THE RECURSION METHOD

In the previous section, we outlined the setting up of the Hamiltonian matrix for an arbitrary assembly of Si atoms, and showed that solving Schrödinger's equation to obtain the density matrix would provide enough information to calculate bond orders, orbital occupation numbers and inter-atomic forces. In this section, we indicate how Schrödinger's equation may be solved in practice.

As mentioned, if the solid has three-dimensional periodicity, the Hamiltonian may be constructed from only the atoms in one unit cell by multiplying its entries by wavevector-dependent Bloch phases. Then the eigenvalues and eigenvectors must be found for all wavevectors, $\mathbf{k}$, in the Brillouin zone. Successive approximations to the exact answer may be obtained by sampling more and more of the infinite values of $\mathbf{k}$. This is the procedure adopted by Chadi in his pioneering work on the atomic structure of semiconductor surfaces [19] and a (221) symmetrical tilt boundary in Si [18]. Since crystal defects are not three-dimensionally periodic, it is necessary in this approach to impose such periodicity by building a supercell of defects. This is the procedure frequently adopted in self-consistent total energy calculations of crystal defects. There is a different method of solving Schrödinger's equation which does not require periodicity, namely Haydock's recursion method [44], and which is popular in semi-empirical calculations of defects [45]. This is the scheme we have adopted for our inter-atomic force calculations. Rather than giving full details of the recursion method, which have appeared frequently elsewhere [e.g. 46], we shall outline the underlying structure of the method and indicate in which respects our implementation differs from that of other authors.

In order to calculate density matrix elements between a number of atoms occupying a small region

of the atomic assembly, instead of making successive approximations in reciprocal (**k**-) space, we can make successive approximations in real-space by solving Schrödinger's equation for successively larger clusters of atoms neighbouring the atoms in question. The advantage of this approach is that quantities such as inter-atomic forces between two atoms will be mostly determined by the disposition of atoms in the neighbourhood of where the force is acting. Therefore for each inter-atomic force the Hamiltonian need be set up only for a cluster of atoms surrounding an atom pair rather than for a whole supercell unit; *this means that larger numbers of non-equivalent atoms can be treated in the recursion method.* One can show [47] that by taking successively larger clusters, the solutions to Schrödinger's equation must converge to the exact result. In contrast to the **k**-space approach, the recursion method does not calculate the eigenvalues and eigenvectors of the Hamiltonian. Indeed these are available only if the Hamiltonian for the whole assembly is set up. Instead, the quantity that is directly approximated is the local density of states (LDOS),

$$n^{i\alpha,j\beta}(E) = \sum_{\substack{n \\ (\text{occ.})}} c_n^{i\alpha} \bar{c}_n^{j\beta} \, \delta(E - E_n) \qquad (3.1)$$

which must be integrated to the Fermi energy, E_f, to obtain the required density matrix element

$$\rho^{i\alpha,j\beta} = 2 \int_{-\infty}^{E_f} n^{i\alpha,j\beta}(E) \, \mathrm{d}E. \qquad (3.2)$$

The degree of approximation to which the density matrix elements are calculated is the "number of recursion levels" which is the number of neighbour shells surrounding atoms i and j. The thickness of each neighbour shell is the range of the off-diagonal Hamiltonian matrix elements, i.e. between first and second neighbour distances in the perfect crystal. The details of the calculation are as follows. We wish to calculate the density matrix elements connecting all orbitals on atom i with all those on atom j [these will enter equation (2.6) for the force acting on atom i due to atom j)]. We decide on the number of levels, L, to use, based on the degree of accuracy required and available computing time, and construct a roughly spherical cluster of atoms about the central pair. This cluster will consist of L neighbour shells to the i–j pair, and we know that in this calculation the first $2L + 1$ power moments of the densities (3.1) will be exactly reproduced. These power moments are

$$\mu_r^{i\alpha,j\beta} = \int_{-\infty}^{\infty} E^r n^{i\alpha,j\beta}(E) \, \mathrm{d}E, \quad r = 0, 1, 2, \ldots$$

Each successive power moment may be calculated using only the Hamiltonian matrix elements that connect atoms i and j to each successive neighbour shell. This is Friedel's moment theorem [48]. (The power moments are none other than the moments of a distribution [49] as encountered in, for example, first and second moments of area of a cross-section in mechanical problems.) In order to calculate the densities (3.1), note that if there are N atoms in the spherical cluster, the Hamiltonian matrix will have dimensions $Nm \times Nm$, where m is the number of orbitals per atoms (four in the present instance). An $Nm \times m$ state vector (an m-column matrix) is set up whose m columns are the starting vectors of the usual "scalar" recursion method [34]. L successive operations of the Hamiltonian matrix on this state vector produce new state vectors which after normalisation and orthogonalisation to each other become a new set of m-column matrix basis functions in which representation the Hamiltonian matrix is block tridiagonal [50]. It is then possible to obtain a $2m \times 2m$ matrix of densities (3.1) for all the α and β-orbitals on the two atoms i and j, by using the matrix entries in the block tridiagonal Hamiltonian as coefficients in a three-term recurrence for matrix orthogonal polynomials. Complete details of this procedure can be found in refs [6, 51–53]. Important advantages of the simultaneous recursion described here are that the interatomic forces are directly obtained from non-diagonal matrix elements and that they are constrained to be *rotationally invariant* which is not necessarily the case in scalar recursion [52].

Integration of the densities, $n^{i\alpha,j\beta}(E)$, can be done simultaneously, rapidly and to arbitrary accuracy using a Gauss–Chebyshev integration method due to Nex [54]. It is worthwhile to make a few remarks about the upper integration limit, the Fermi energy, in connexion with the charge neutrality condition. In Chadi's method [18, 19], the orbital energies, ϵ_s and ϵ_p are constants so that as the atoms move and LDOS's change, the number of electrons on each atom will vary. In order to conserve the total number of electrons in the supercell, at each iteration of the relaxation algorithm, the Fermi energy must be adjusted and when the Hamiltonian is diagonalised to obtain density matrix elements some charge transfer will, in general, be found. This adjustment can only be made in a **k**-space, supercell method. In the recursion method without charge neutrality, either global charge conservation must be violated or the Fermi level must change from site to site (a very unphysical situation). With the charge neutrality condition, all atoms, by construction, have an equal number of electrons and the Fermi level is fixed by its value in the perfect crystal. In this situation one can think of the defect as properly embedded in an infinite perfect crystal which supplies a bath of electrons with a fixed chemical potential. Further embedding of the cluster is provided in the recursion method using a "terminator". But this is a technical matter and does not affect the formal convergence properties [47, 55].

Besides binding energies and interatomic forces, it is possible using the diagonal densities (3.1) to examine the local electronic structure as reflected in on-site local densities of states. This provides a

"fingerprint" of the defect or perfect crystal and indicates how the local electronic structure is perturbed at a defect by the appearance of resonances in the energy bands or bound states in forbidden gaps. Thus the method we have adopted is internally consistent in the sense that all the quantities we wish to calculate, forces, energies and densities of states are determined using the same method. This is not usually the case in atomistic simulations [46].

4. APPLICATIONS AND EXAMPLES

The calculations, while quantum mechanical in origin, are not obtained from a self-consistent solution of Schrödinger's equation with the Hamiltonian expressed in a complete, orthogonal basis. The incompleteness arises from the use of a minimal basis (that is, s and p electrons only); non-orthogonality is approximately corrected for using an inverse fourth power repulsive pair potential, $\varphi(r) = A/r^4$. The parameter, A, is adjusted so that the equilibrium condition is satisfied, or in other words, to obtain the observed lattice parameter in crystalline Si. Therefore, rather in the spirit of the development of classical interatomic potentials, it is necessary to apply a number of tests to the model to ensure that it provides an adequate description of solid Si. In this section, we show the results of these tests, and at the same time illustrate the usefulness of the description of the binding energy in terms of density matrix elements.

4.1. Tests on perfect crystals: structural stability

The pair-potential used by Chadi in his work [18, 19] has three parameters which are fitted to the lattice constant, bulk modulus and cohesive energy of Si. Since our pair potential has only one parameter, we can use the model to calculate the bulk modulus and cohesive energy [6]. Taking into account the spin-polarisation energy (see Section 8.2) the cohesive energy in our model is 3.94 eV/atom and the experimental value is 4.70 eV/atom. The bulk modulus is not as well reproduced: from just ten moments it is underestimated by about $\frac{2}{3}$, whereas a converged calculation underestimates it by about $\frac{1}{2}$. As discussed in Section 8.2 these results can be improved either by using an inverse fifth power in the pair potential, or by fitting the bulk modulus directly. In the latter option, it is then found that the model reproduces the other elastic constants with good accuracy [56] and the experimental phonon dispersion relations are well reproduced [57].

It is most important that the model correctly predicts the phase stability of Si. We show, in Fig. 1, energy–volume curves for Si in five different crystal structures, which we compare with accurate quantum-mechanical calculations [58].

It is immediately obvious, that the energies of non-tetrahedrally bonded structures are only poorly predicted by the model. However, it is reassuring that

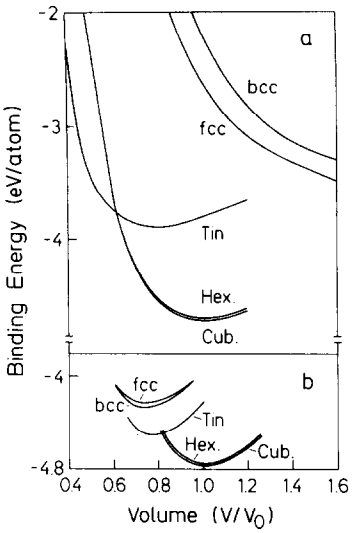

Fig. 1. Binding energy–volume curves for five crystal structures of Si: f.c.c.—face centred cubic; b.c.c.—body centred cubic; Tin—β-tin; hex—hexagonal diamond; cub—cubic diamond. (a) Computed in the tight binding model with a $1/r^4$ repulsive pair potential [6]. (b) The same curves obtained by density functional theory [58].

the close packed structures are higher in energy than diamond and hexagonal diamond; this is a consequence of the inverse square scaling of the bond-integrals. If they scale more steeply, as for example in work by Pandey and Phillips [59] who used an inverse sixth power scaling at first-neighbour distance, then it is found that the close packed structures are much lower in energy than the diamond phases [6]. Note that the model correctly predicts the energy difference between the cubic and hexonagonal diamond structures. These are not distinguished by using many classical potential descriptions of Si [e.g. 60].

By considering the band energy alone, it is possible to obtain some insight into the phase stability of the competing phases. Here we will briefly demonstrate this in order to illustrate the use of the density matrix elements in interpreting the interplay between atomic and electronic structure. For details, we refer the reader to Ref. [53]. The binding energy (2.4) may be re-cast [6] into the form

$$E_B = E_{cov} + E_{site} + E_{rep} + \text{constant}.$$

The constant is equal to $-2N(\epsilon_s + \epsilon_p)$, where ϵ_s and ϵ_p contain the crystal field terms. E_{site} contains the diagonal terms in the band energy (2.3a) that were pulled out in writing E_{cov}

$$E_{site} = \sum_{i\alpha} \rho^{i\alpha, i\alpha} H_{i\alpha, i\alpha}.$$

Now, leaving out the repulsive energy, the binding energy can be seen to break down into contributions from products of partial bond orders and bond integrals (bond contributions), and terms relating to the redistribution of electrons between the different orbitals on one site (hybridisation contributions). The

Table 1. Breakdown of the hexagonal–cubic diamond energy difference [53]. All energies in eV

Structure	Band energy	s–p mixing		$B_{ss\sigma}$	$B_{sp\sigma}$	$B_{pp\sigma}$	$B_{pp\pi}$
Cubic	−20.993	1.71		−0.812	−2.479	−4.245	−0.603
hexagonal	−20.981	1.73	A	−0.827	−2.485	−4.261	−0.607
$c/a = \sqrt{(8/3)}$			B	−0.821	−2.507	−4.211	−0.561

best way to see this is to write out E_{cov} in full for one bond (between atoms i and j), after first rotating the coordinates so that the bond in question points along the z-axis

$$E^{ij}_{cov} = 2[\rho^{is,js}V_{ss\sigma} + (\rho^{is,jz} - \rho^{iz,js})V_{sp\sigma} + \rho^{iz,jz}V_{pp\sigma} + (\rho^{ix,jx} + \rho^{iy,jy})V_{pp\pi}] \equiv B_{ss\sigma} + B_{sp\sigma} + B_{pp\sigma} + B_{pp\pi}.$$

Here, x, y and z refer to the p_x, p_y and p_z orbitals. The factor of 2 arises from equal i–j and j–i contributions in the sum in equation (2.5). We see that the covalent bond energy contribution from each individual bond can be characterised by four *partial bond energies*. The site energy contribution from atom i can be written simply as

$$E^i_{site} = \rho^{is,is}\epsilon_s + (\rho^{ix,ix} + \rho^{iy,iy} + \rho^{iz,iz})\epsilon_p$$

and this can be characterized by a single parameter

$$(\rho^{ix,ix} + \rho^{iy,iy} + \rho^{iz,iz})/\rho^{is,is} \equiv N^i_p/N^i_s$$

which we have called [6] the *s–p mixing* on site i. It is simply the ratio of the occupation of p orbitals to the occupation of s orbitals; if, in forming the solid from free atoms an electron in an s-state is promoted into a p-state the s–p mixing will be 3. Note that the assumption of an sp^3 basis does not impose automatically an s–p mixing of 3. The s–p mixing depends on the atomic environment even though the basis is fixed.

As an illustration, we will discuss the relative stability of the cubic and hexagonal diamond phases [53]. Each structure has atoms with four neighbours, all the bond lengths being the same if the axial ratio of the hexagonal phase is ideal. Then in calculating energy differences, the repulsive energies cancel, and we need only consider the differences in covalent bond and site energies. The cubic diamond structure has all bonds equivalent. In hexagonal diamond, there are three equivalent bonds related via 6-fold rotation symmetry parallel to the c-axis and a fourth bond parallel to the c-axis which is not related to these by symmetry. They will be denoted bonds A and bond B respectively. Table 1 shows the band energies (eV/atom), the s–p mixing and partial covalent bond energies (eV/bond) of the non-equivalent bonds.

The energy difference between hexagonal and cubic diamond is 0.01 eV/atom (about 1 kJ/mol). However, the A-bonds in the hexagonal structure are stronger (in the sense that they contribute a more negative covalent bond energy) than the bonds in the cubic phase. The B-bonds are weaker, but the total covalent bond energy is more negative in the hexagonal phase. The structure is less stable because by forming stronger bonds it has had to promote more s electrons into p orbitals to increase the s–p hybridisation. The s–p splitting is about 5 eV so the energy penalty is considerable. This increased hybridisation is reflected in the s–p mixing. Note that rather than being 3, the s–p mixing in both structures is about 1.7, indicating that the bonds are not formed from complete sp^3 hybrids as originally suggested by Coulson [27].†

We should point out that if the s–p mixing is 1, as found in Si in close-packed phases [6], although there is no penalty from s–p promotion, there is also almost no benefit gained from bond formation and the solid will have little cohesive energy with respect to the free atoms. The picture obtained from the comparison of cubic and hexagonal diamond structures shows the subtle balance between site and bond contributions. The surprising result is that the cubic structure is more stable, not by forming stronger bonds, but by optimising the balance between energy gained by bond formation and energy lost through s–p promotion.

4.2. *Tests on simple defects: stacking fault and twin interface*

We now turn to two of the simplest interfaces in Si, the intrinsic stacking fault and the (111) symmetrical tilt boundary which is the interface observed between deformation twins [62]. They are discussed in this section firstly because calculation of stacking fault energy provides a useful check of the model by comparing with experiment, and secondly because although these structures were relaxed, no significant atom movements occurred from ideal crystal positions; therefore we can discuss the stacking fault and twin interface before describing the relaxation method. Also in this section, we describe the method of displaying densities of states and calculating boundary energies.

4.2.1. The density of states. The local density of states (LDOS) associated with atom i is

$$n^i(E) = \sum_\alpha n^{i\alpha,i\alpha}(E). \qquad (4.1)$$

†Diamond carbon, which may be expected to show complete sp^3 hybridisation because of its large band gap (about 6 eV, compared to 1.2 eV in Si), has an s–p mixing of 2.3 using Harrison's [16] tight-binding parameters. Second neighbour Hamiltonians give what may be more realistic figures: in Si, 2.1 [6]; in C, 2.6 (using a second neighbour two-centre fit to the band-structure of Ref. [61]). We are grateful to Dr A. M. Stoneham for suggesting this comparison and Dr P. Pecheur for providing the parameters for diamond carbon.

In a crystal with all atoms equivalent, any atom, i may be chosen. In the recursion method, a cluster of 3000–4000 atoms in the shape of a cube is constructed around this atom and a scalar tridiagonal Hamiltonian is calculated to 40 levels, about the first 15 of which will be exact and the rest approximated in the sense that they will contain effects due to the cube's surfaces. The advantage of this method is that the resolution of features in the density of states is of the order of 1/40 of the energy spectrum (about 20 eV), while the number of atoms is kept to a minimum. The disadvantage is that the effect of the surface is to introduce some spurious structure in the density close to the two extremal band edges. The density of states is calculated using Nex's gaussian quadrature method [47, 63].

Figure 2 shows the density of states of Si in the cubic and hexagonal diamond structures. Note the clear separation betweeen valence and conduction bands, and absence of the middle valence band peak in the hexagonal diamond density of states.

4.2.2. Grain boundary energy. In order to calculate the energy of a relaxed grain boundary, we sum contributions to the binding energy (2.4) from all non-equivalent atoms in the bicrystal. For each atom, the binding energy it would contribute in the perfect crystal is subtracted and the boundary energy is obtained by dividing by the area of the unit cell in the boundary plane. The band energy can be calculated in one of two ways as can be seen from equation (2.3). Using (2.3a) we need both diagonal and non-diagonal density matrix and Hamiltonian matrix elements, and this is called the Inter-site Method (ISM); using (2.3b) (which can be evaluated on each atom by multiplying the density of states $n^i(E)$ by E and integrating to the Fermi energy with respect to E) requires only diagonal matrix elements and is called the Site-diagonal Method (SDM). Formally (2.3a) and (2.3b) are identical but, in the recursion method, limiting the calculation to a finite number of levels will give different answers which will both converge to the correct result by using more levels. Comparing the two values for a given number of levels then gives an indication of the error arising from a finite number of recursion levels. In the ISM, we get a rather transparent expression for the binding energy in terms of contributions from the bonds

$$E^{ij}_{\text{bond}} = E^{ij}_{\text{cov}} + E^{ij}_{\text{rep}}$$

and on-site contributions

$$E^i_{\text{site}} = \sum_\alpha \rho^{i\alpha, i\alpha} H_{i\alpha, i\alpha} = \sum_\alpha n^i_\alpha(\epsilon_\alpha + \Delta_i)$$

where Δ_i are the increments to the ϵ_α that ensure local charge neutrality (Section 2.3). The contribution to the binding energy from site i is

$$E^i_{\text{B}} = \tfrac{1}{2} \sum_{\substack{j \\ \text{neighbours}}} E^{ij}_{\text{bond}} + E^i_{\text{site}} - 2(\epsilon_{\text{s}} + \epsilon_{\text{p}}).$$

In this expression, the first term is simply the sum of energies of bonds to atom i divided by 2 since each bond energy may be associated with atom i and atom j. The second term identifies the site energy as essentially non-pairwise and strongly affected by the charge neutrality condition. The third term is a constant. We emphasize that both of the first terms are strictly many-body quantities since they are dependent on the atomic environments surrounding atom i and its neighbours.

4.2.3. Stacking fault and twin interface. Figure 3 shows the atomic structures of the intrinsic stacking

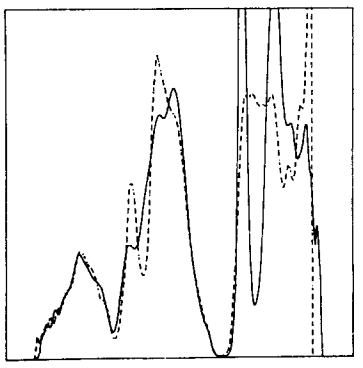

Fig. 2. Density of states in the hexagonal diamond structures of Si (full line) and cubic diamond structure (broken line) computed in the tight binding model to 40 recursion levels and using gaussian quadrature.

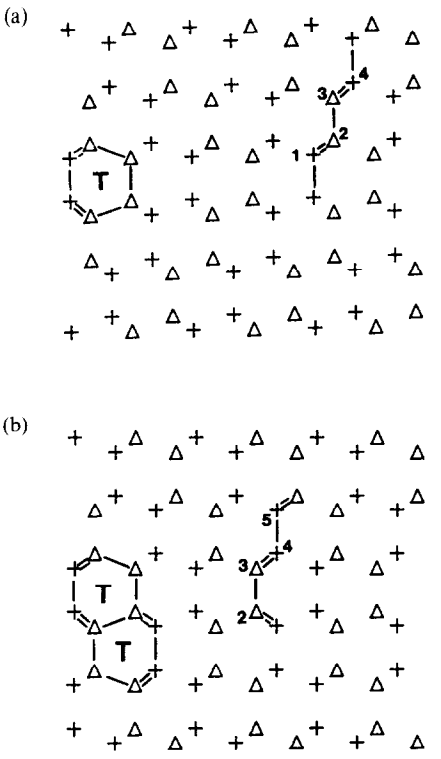

Fig. 3. (a) Relaxed (111) symmetrical tilt boundary in Si. (b) Relaxed intrinsic (111) stacking fault in Si. Triangles and crosses represent atom positions on successive (2$\bar{1}$0) planes along the [1$\bar{1}$0] projection direction, which is normal to the page. T labels a twin unit. Local densities of states for atoms labelled in this figure are given in Fig. 4.

fault and (111) symmetrical tilt boundary in Si projected onto the $(1\bar{1}0)$ plane.

The letter T labels the twin units that exist in both these boundaries and which have been denoted 6_b by Papon and Petit [15] in their extensive tabulation of structural units in cubic diamond lattices. These are units of the hexagonal diamond lattice; and just as in the f.c.c./h.c.p. transformation, the cubic diamond lattice may be transformed into the hexagonal by the introduction of an intrinsic stacking fault on every second (111) lattice plane. This was pointed out by Tan *et al.* [64] who estimated the energy difference between hexagonal and cubic diamond Si form the measured stacking fault energy (60 mJ/m^2) and found 0.017 eV/atom which is close to the 0.01 eV/atom found in both our empirical tight-binding method and also a fully self-consistent quantum mechanical calculation [65]. It is remarkable that such a simple estimation based on the transfer of 6_b units into the cubic diamond lattice should be so successful. In Fig. 4, we show the local density of states, equation (4.1), on the atoms labelled in Fig. 3.

By comparing with Fig. 2, there is a striking resemblance between the densities of states of atoms in the stacking fault and in the hexagonal diamond structure. Whereas the stacking fault consists of two layers of twin units, the twin interface has just a single layer of these. Therefore there are atoms in the stacking fault bounded by two 6_b units, e.g. atom 2 of Fig. 3(b), (which show the greatest similarity to the hexagonal diamond atoms), and atoms which are bounded by a cubic diamond 6 unit [15] on one side and a 6_b unit on the other, e.g. atom 3 of Fig. 3(b). The latter have a density of states resembling atoms in the twin interface, e.g. atom 1 of Fig. 3(a), since in this case, there being only one layer of 6_b units, they have similar atomic environments. It is clear from this that the local electronic structure is to a very large extent governed by the local atomic structure extending to just a few neighbour shells; which demonstrates the value of the recursion method in calculating interatomic forces. It demonstrates also the usefulness of a structural unit description of a grain boundary by identifying characteristic atomic environments for which the LDOS's are already known.

Because the energies of the stacking fault and twin interface are so small their calculation represents a considerable challenge to any computation based on electronic structure considerations. The energies of the stacking fault and twin interface calculated by the recursion method are shown in Table 2. We indicate the number of recursion levels, L, in each calculation, the number of atoms in the recursion cluster (to give an idea of the size of the spherical clusters) and the energy obtained in the ISM and SDM (see Section 4.2.2).

We were not surprised to find that using fewer than six levels the energies were negative. This is also the case for the hexagonal–cubic diamond energy difference which has the right sign only when more than four levels are used [53]. Just as in pair potential determinations of stacking fault energies in Al [66] the results are poorly converged as a function of the size of the region explicitly included in the calculation. (Note that a fully self-consistent calculation gives 40 mJ/m^2 [67] which is also in rather poor agreement with the experimental value.) Fortunately as shall be seen in Section 6, boundaries with higher energies give much better results. Also numerical tests have shown that interatomic force calculations converge faster than grain boundary energies (Section 6). The rather poor agreement between SDM and ISM determinations indicates a lack of convergence even at 8 levels. Based on the success of Tan *et al.*'s estimate of the hexagonal–cubic energy difference, and noting that the twin interface comprises exactly half the number of 6_b units as the stacking fault, we expect its energy to be half that of the stacking fault. This is also seen in Table 2 if results using the same method and numbers of levels are compared. This shows that grain boundary energy differences converge much faster than absolute grain boundary energies, and emphasises the importance of allowing systematic errors to cancel in electronic structure calculations [23, 34, 53, 58]

Table 2. Stacking fault and twin interface energies (mJ/m^2)

		Stacking fault		Twin interface	
L	No. of atoms	SDM	ISM	SDM	ISM
6	239	88	120	43	62
7	363	123	169	54	71
8	525	115	77	56	29

5. METHOD OF GRAIN BOUNDARY RELAXATION

The enthalpy at 0 K of a unit cell containing a single grain boundary between two floating perfect crystals is minimized. The periodicity of the bicrystal parallel to the boundary plane is exploited to generate the positions of atoms in other unit cells as they are needed. No periodicity along the boundary normal is assumed and the bicrystal is therefore of finite size in that direction. Initially, a thin block of material (about 1 crystal lattice parameter thick) centred on and parallel to the boundary is relaxed, allowing the "sub-blocks" of material on either side to float rigidly parallel and perpendicular to the boundary. The relaxed region is then expanded by three atomic layers on either side of the boundary and re-relaxed. This is repeated until no further relaxation occurs on increasing the size of the relaxed region. It is ensured that all the material in the relaxed region is completely unaffected by the free surfaces at the ends of the unit cell normal to the boundary. This means that it must not be possible for an electron to hop from the relaxed region to a free surface during the

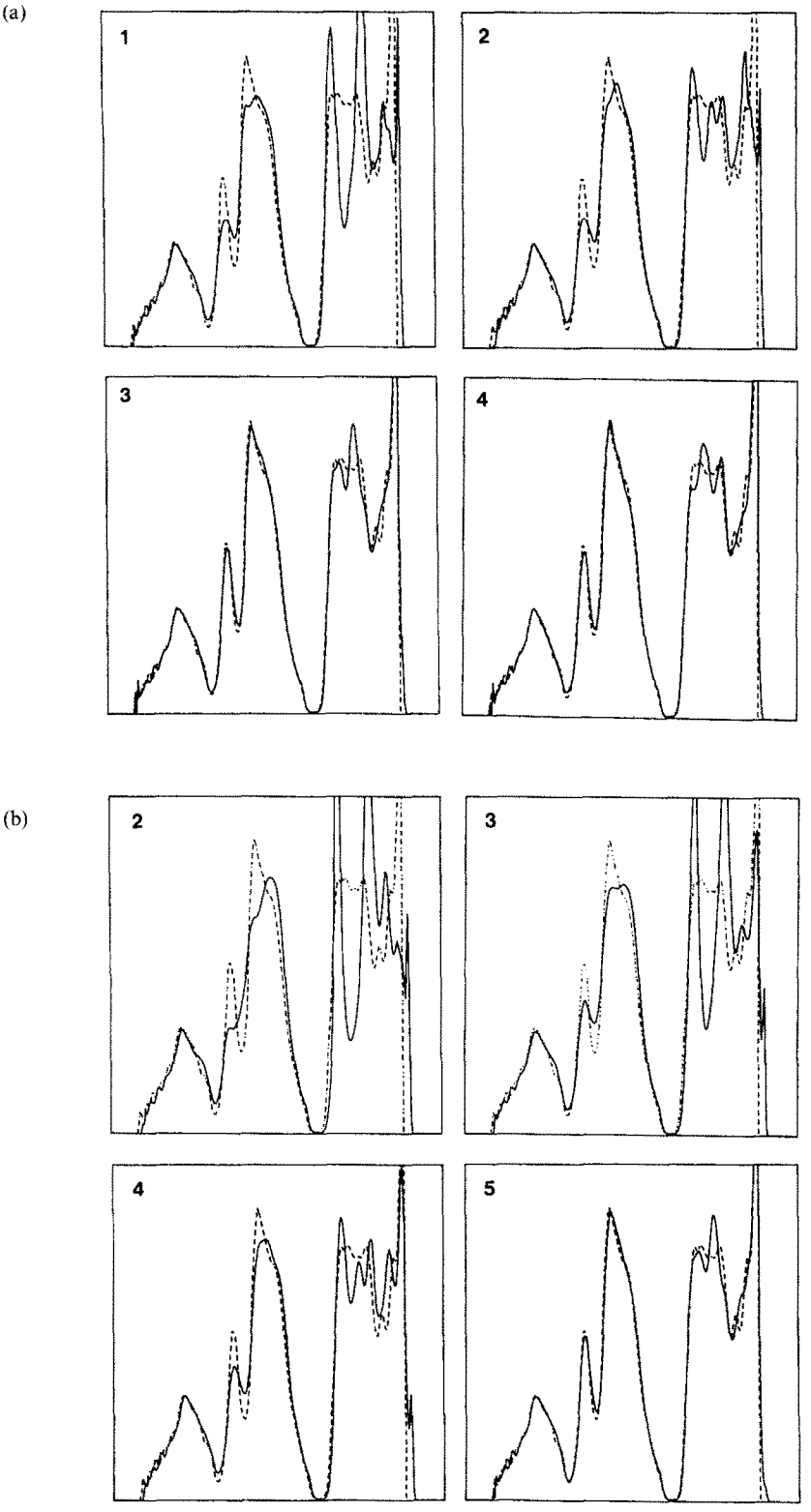

Fig. 4. (a) Local densities of states at atoms labelled in Fig. 3 (a). (b) Local densities of states at atoms labelled in Fig. 3 (b). In this and subsequent figures the broken lines show the local density of states in the perfect diamond cubic crystal.

operation of the recursion method. The final result is thus a single relaxed grain boundary of effectively infinite extent parallel to the boundary plane which is not subjected to any macroscopic stress normal or parallel to the boundary plane. The rigid body relative translation vector, **t**, of one grain relative to the other is determined simultaneously with the local atomic relaxation. If N_a is the number of atoms in the relaxed region of the unit cell at some time then the number of variables in the energy minimization is $v = 3N_a + 3$, the last three being the ralative translation vector, **t**.

The time consuming step is the evaluation of interatomic forces by the simultaneous recursion method outlined in Section 3. Therefore it is essential to minimise the number of evaluations of the force, equation (2.6), acting on one atom due to another. This is one reason why we have chosen not to use molecular dynamics. For the same reason we have used a variable metric minimisation routine developed at Harwell and applied by Tasker and co-workers [68] in their studies of surfaces and grain boundaries in ionic crystals. Variable metric minimisation methods are well documented [69]. It suffices to note here than the Harwell routine updates and improves a stored v by v Hessian matrix using only the v forces of the current and previous iterations and the Hessian matrix of the previous iteration. The Hessian is the inverse of the matrix of second derivatives of the energy with respect to the v variables. It is initially set equal to a constant diagonal matrix and it is updated in subsequent iterations without having to evaluate any second derivatives or matrix inversions. We have found that convergence is faster and more complete with this energy minimization method than with steepest descent and conjugate gradient methods. (Wolf [70] found similar results with his method which involved the evaluation of the exact Hessian matrix at each iteration.) The disadvantage with the variable metric method is that one has to store a symmetric $v \times v$ matrix. In this work the largest number, v, of variables we have treated is 987. In our code treating defects with such large numbers of associated relaxation variables is made possible by the fact that we store the positions of only non-equivalent atoms in the bicrystal. The positions of atoms in clusters that are required to operate the recursion method to a given number of levels are generated when they are needed from the non-equivalent atom positions and the periodicity parallel to the boundary.

6. (11$\bar{2}$) SYMMETRICAL TILT GRAIN BOUNDARY IN Si

6.1. *Review of experimental observations*

High resolution electron microscopy observations by Bourret *et al.* [10] on the (11$\bar{2}$) symmetrical tilt boundary in Ge have shown that this boundary has double the normal coincidence site lattice periodicity in the boundary plane along [111]. Electron diffraction experiments by Petit, which were reported by Bourret and Bacmann [71], confirm this result and furthermore show that the period along the [1$\bar{1}$0] direction is also doubled relative to the coincidence site lattice. Moreover the diffraction pattern indicated that the two dimensional repeat cell in the boundary is centred and has *cm* symmetry. We adopt the notation from surface science [e.g. 72] that the boundary periodicity is indicated by $(n \times m)$, meaning that the unit cell is bounded by n[111] and $m/2$[1$\bar{1}$0]. Thus the boundary has *cm* (2 × 2) symmetry. The rigid body translation in Si was measured [73] by the α-fringe technique and found to be 0.07–0.09 [111], 0.05–0.07 [11$\bar{2}$]. In Ge the translation was determined [10] directly from the high resolution images and found to be 0.08–0.10 [111], 0.03–0.06 [11$\bar{2}$]. In [10, 73, 74] no translation along [1$\bar{1}$0] was detected which is consistent with there being a mirror plane perpendicular to that direction. The translation state quoted for Si by Fontaine and Smith [74] was not consistent with their model [75]. Papon and Petit proposed [15] a *pm* (1 × 2) reconstruction for the (11$\bar{2}$) boundary before it was established experimentally that the symmetry is *cm* (2 × 2). In each [111] period of the *pm* (1 × 2) structure there are two [1$\bar{1}$0] rows of atoms along which successive pairs of atoms are pinched together and bonded in a similar fashion to the reconstruction proposed for 30° partial dislocations [76]. This doubles the period along [1$\bar{1}$0]. Bourret *et al.* [10] noted that a centred (2 × 2) reconstruction could be generated very easily from the (1 × 2) structure by shifting the reconstructed [1$\bar{1}$0] rows in alternate [111] periods by $\frac{1}{2}$[1$\bar{1}$0]. Those authors obtained good overall agreement between the simulated and experimental structure images with their *cm* (2 × 2) structure although there was a region where the agreement was poor.

6.2. *Results*

In this work we have considered five metastable structures for the (11$\bar{2}$) boundary in Si. All of these structures were proposed as suitable reconstructions by other authors and we have included the *pm* (1 × 2) [15] and *cm* (2 × 2) [10] reconstructions. Table 3

Table 3. Summary of results for the 5 reconstructions of (11$\bar{2}$) symmetric tilt boundary in Si

Source of reconstruction	Periodicity units of [111] × $\frac{1}{2}$[1$\bar{1}$0]	Relaxed Shubnikov layer group	Calculated translation state			Energy (mJ/m^2)
			[111]	[11$\bar{2}$]	[1$\bar{1}$0]	
[77]	(1 × 1)	*p2′mm′*	0	0.013	0	1200 ± 80
[79]	(1 × 1)	*p2₁mn′*	0.167	0.056	0.25	670 ± 20
[11]	(1 × 2)	*p2′mm′*	0	0.023	0	450 ± 20
[15]	(1 × 2)	*pm*	0.092	0.032	0.24	350 ± 30
[22]	(2 × 2)	*cm*	0.092	0.032	0.25	340 ± 30

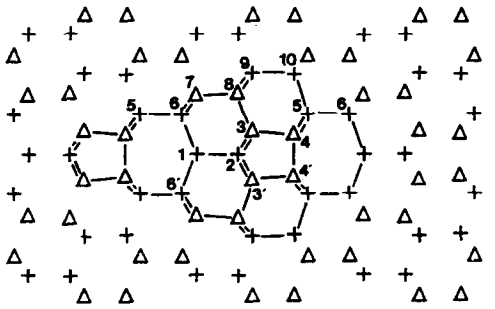

Fig. 5. Relaxed structure of $p2'mm'$ (1×1) $(11\bar{2})$ symmetrical tilt boundary in Si. The boundary plane passes through atoms labelled 1 and 2. Atoms labelled n and n' are related by symmetry.

contains a summary of the relaxed structures we have obtained for this boundary.

As we have already remarked in Section 4.2.2 the degree of convergence of the energy calculation can be ascertained by comparing the ISM and SDM evaluations of the energy. The energies given in Table 3 were computed to 8 exact levels in the recursion method and a conservative estimate of the degree of convergence is indicated after each energy. The convergence of the relaxed atomic structure was also tested numerically by comparing the pm (1×1) structure computed to 4 and 6 levels. The maximum difference of any atomic coordinate was found to be less than 0.04 Å. We conclude that the atomic structure converges more rapidly than the boundary energy with number of exact recursion levels. This is the reason why we computed the boundary energies with eight exact levels.

The highest energy structure, $p2'mm'$ (1×1), was proposed as a low energy structure by Möller [78], who obtained a boundary energy of 1760 mJ/m^2 by a valence force field relaxation. (We note that the energy of this boundary was given incorrectly in [7] as 2700 ± 80 mJ/m^2.) It is interesting because it contains three and five fold coordinated atoms as seen in Fig. 5 at atoms labelled 1 and 2.

Seven layers on either side of the boundary were relaxed so that there were 28 non-equivalent atoms in the computational cell. The maximum residual force on any atom was 0.007 eV/Å. Changes in individual covalent bond energies (computed to 8 levels) and percentage changes in bond lengths are shown in Table 4.

Table 5. Changes in the on-site Hamiltonian matrix elements, Δ_i, the site energies ΔE_{site}, and the s–p mixing Δs–p mixing, all relative to the perfect crystal for atoms labelled in Fig. 5

Atom number	Coordination	Δ_i (eV)	ΔE_{site} (eV/atom)	Δs–p mixing
1	3	−0.585	−3.084	−0.203
2	5	0.286	1.216	0.020
3	4	0.386	1.036	−0.132
4	4	0.092	0.429	0.016
5	4	−0.112	−0.436	0.003
6	4	−0.323	−1.370	−0.023
7	4	−0.152	−0.681	−0.020
8	4	0.066	0.327	0.018
9	4	−0.005	−0.006	0.005
10	4	−0.046	−0.212	−0.009

Deviations from the ideal bond angle (109.47°) vary between −40 and +31%. Table 5 summarizes the changes in the site energies, ΔE^i_{site}, the changes in the s–p mixing, the changes Δ_i in the on-site Hamiltonian matrix elements to achieve local charge neutrality to 9 exact levels and 10^{-4} electrons/atom tolerance, and the local coordination number. These changes are all relative to the perfect crystal.

It is seen that atom number 1, which is three fold coordinated, has a large negative change in its site energy caused both by rehybridisation, reflected in the reduction in the s–p mixing (less sp^3 like, more s^2p^2 like), and by a large negative shift, Δ_i, in its on-site Hamiltonian matrix elements. The covalent bond it forms with the five fold coordinated atom, number 2, is stronger than in the perfect crystal, due to the contraction in the bond length. The ppπ bonding between atom 1 and its 3 neighbours has been enhanced as seen by the negative values of $\Delta B_{pp\pi}$, in spite of an increase in the bond length between atoms 1 and 6. It is clear that although atom 1 is only 3 fold coordinated it has optimised its energy by rehybridisation, changing the electronic character of the bonds it is able to form. It would therefore be invalid to assign a dangling bond energy to this atom equal to half the energy of a bond in the perfect crystal. Turning to the five fold coordinated atom it is noted that four of its bonds are stretched by 5.6% resulting in covalent bond energies 1.913 eV higher than in the perfect crystal. Its site energy is also raised primarily because the on-site Hamiltonian matrix elements are shifted upwards in energy. The Δ_i's show that if local charge neutrality had not been imposed there would have been a substantial flow of electronic charge from atoms 1, 6 and 6′ to atoms 2 and the four

Table 4. Changes in covalent partial bond energies (eV) and bond lengths between atoms labelled in Fig. 5, relative to the perfect crystal

Atom numbers	$\Delta B_{ss\sigma}$	$\Delta B_{sp\sigma}$	$\Delta B_{pp\sigma}$	$\Delta B_{pp\pi}$	ΔE_{bond}	Δl(%)
1, 2	−0.001	−0.097	−0.369	−0.391	−0.857	−2.990
1, 6	0.031	0.069	0.348	−0.253	0.194	1.532
2, 3	0.150	0.631	1.007	0.126	1.913	5.649
3, 8	−0.006	−0.090	−0.356	−0.153	−0.606	−2.810
3, 4	0.032	0.136	−0.268	−0.095	−0.195	−0.019
4, 4	−0.289	0.002	0.241	0.178	0.232	0.457
4, 5	−0.044	−0.059	−0.010	−0.019	−0.131	−0.614
5, 6	−0.003	−0.024	−0.035	−0.016	−0.079	0.566
5, 10	0.020	0.061	0.144	0.028	0.254	1.316

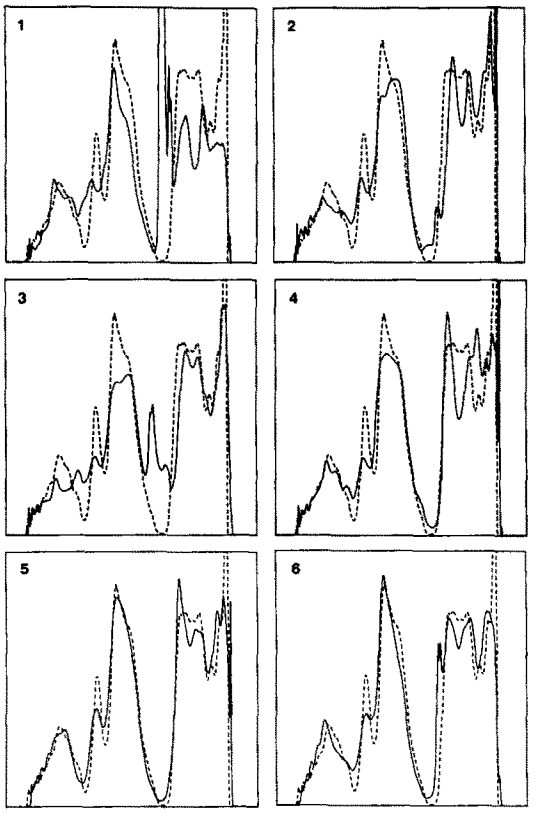

Fig. 6. Local densities of states at atoms labelled in Fig. 5.

atoms at 3 and 3′, i.e. from the 3 fold to the 5-fold coordinated atoms and their neighbours. Intuitively this is what one would expect since atom 1 has one electron more than it can use in bonding whereas atom 2 needs another electron to form 5 bonds. The local densities of states for atoms 1–6 are shown in Fig. 6. A prominent state in the band gap can be identified in the LDOS of the 3 fold coordinated atom, number 1. By contrast the five fold coordinated atom shows little structure in the band gap although its 4 neighbours at 3 and 3′ show more. The LDOS's on atoms 9 and 10 (not shown) are almost indistinguishable from the perfect crystal LDOS, indicating that the boundary perturbs the LDOS's in the adjoining grains to a distance of approximately one lattice parameter on either side.

The $p2_1'mn'$ (1×1) reconstruction has the next highest energy. Vlachavas and Pond [74] found experimentally that the relative translation of the crystals does not correspond to mirror or mirror glide

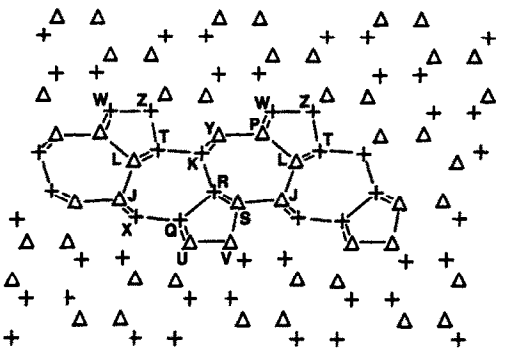

Fig. 7. Relaxed structure of $p2_1'mn'$ (1×1) $(11\bar{2})$ symmetrical tilt boundary in Si. The boundary plane passes between atoms labelled K and R and atoms labelled L and J.

symmetry across the interface. Pond [79] proposed a reconstruction with $p1m1$ symmetry on the basis of these results, which is described particularly clearly in [11]. When we relaxed this structure we obtained the structure shown in Fig. 7, which has $p2_1'mn'$ symmetry. All atoms are four fold coordinated and the structure was relaxed using four recursion levels to a maximum force of 0.006 eV/Å.

The translation component along [111] is slightly different from the relaxed structure obtained by [11] and results in the layer group $p2_1'mn'$ whilst the energy and translation state are in good agreement with Bourret *et al.* [10] who find 600 mJ/m^2 and a translation of $\frac{1}{6}$[111] in plane as well as an expansion of 0.017[11$\bar{2}$]. (We note that the layer group of our relaxed structure was given incorrectly in [7] as *pm*.) The rather high energy of this boundary is attributable mainly to the rather large increases in bond length as seen in Table 6.

In each boundary period there are 6 bonds which have been stretched by more than 8%, each giving an increase in the covalent bond energy of approximately 1.5 eV, which is partially off-set by a decrease in the repulsive pair potential energy. The ppσ and spσ covalent bond energy contributions are most affected by the bond stretching. Table 7 summarizes the changes in the s–p mixing and site energies. The s–p mixing became slightly more s^2p^2 like in the boundary, the changes in the site energies were caused primarily by the self-consistent changes, Δ_i, in the on-site Hamiltonian matrix elements. Apart from atoms J and Y, and the symmetry related atoms K and X, all the Δ_i's were positive, indicating that the boundary had to become more repulsive to electrons

Table 6. Changes in covalent partial bond energies (eV) and bond lengths between atoms labelled in Fig. 7, relative to the perfect crystal

Atoms	$\Delta B_{ss\sigma}$	$\Delta B_{sp\sigma}$	$\Delta B_{pp\sigma}$	$\Delta B_{pp\pi}$	ΔE_{bond}	Δl (%)
L, P	0.144	0.458	0.846	0.177	1.565	8.360
L, J	0.026	0.043	−0.016	−0.036	0.017	0.036
L, T	0.091	0.226	0.333	0.014	0.665	3.272
S, J	0.089	0.315	0.944	0.135	1.483	8.658
S, V	0.009	0.130	−0.308	−0.080	−0.260	−1.531
P, Y	0.118	0.358	0.931	0.105	1.511	8.495
K, Y	0.092	0.161	0.163	0.008	0.424	2.132
P, W	0.036	0.110	−0.058	−0.044	0.043	0.130

Table 7. Changes in Δ_i, E^i_{site}, and s–p mixing for atoms labelled in Fig. 7

Atom	Δ_i (eV)	ΔE^i_{site} (eV/atom)	Δs–p mixing
L	0.185	0.488	−0.072
T	0.200	0.621	−0.051
J	−0.012	−0.246	−0.056
P	0.172	0.425	−0.072
Y	−0.011	−0.307	−0.073
U	0.397	1.629	0.011
V	0.380	1.567	0.011

to maintain local charge neutrality. The bond angles are found to vary from the ideal value between −11 and +26%. LDOS's are shown in Fig. 8.

There are no states deep inside the band gap but there is a suggestion of a bound state associated with the conduction band edge and possibly with the valence band edge but projected band structures would be required to establish this. Bound states at band edges are anticipated in the presence of stretched bonds since the bonding-antibonding splitting is reduced by the weaker hopping integrals. The electronic contribution to the boundary energy is reflected by the skewing over of the LDOS's to higher energies compared with the LDOS of the perfect crystal.

The $p2'mm'$ (1×2) structure, shown in Fig. 9, was also suggested in [11] although it was realised that the experimentally established existence of a relative translation was incompatible with this Shubnikov group.

In agreement with [10] and [11] we find that the energy of this boundary is lower than the energy of the $p2_1'mn'$ (1×1) structure, although the energy 300 mJ/m^2 obtained in [10] is significantly lower than our 450 mJ/m^2. The period doubling along $[1\bar{1}0]$ is caused by pairs of atoms, labelled 3 and 3′ in Fig. 9, pinching together along $[1\bar{1}0]$ and bonding. In this

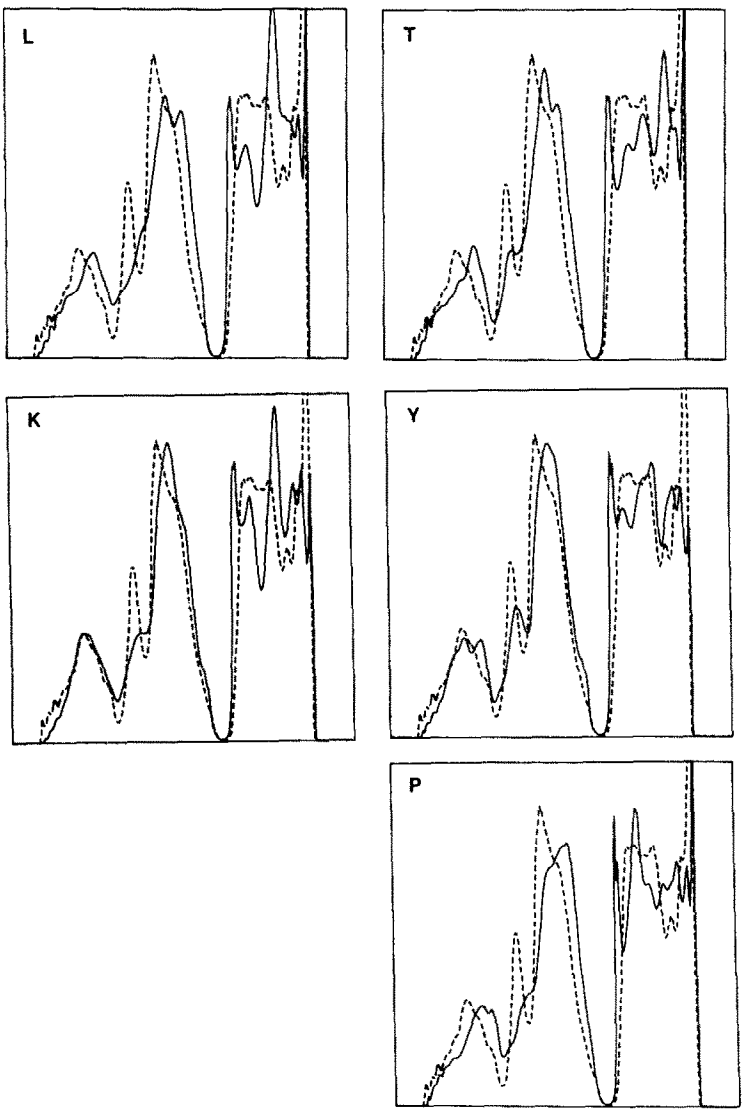

Fig. 8. Local densities of states at atoms labelled in Fig. 7.

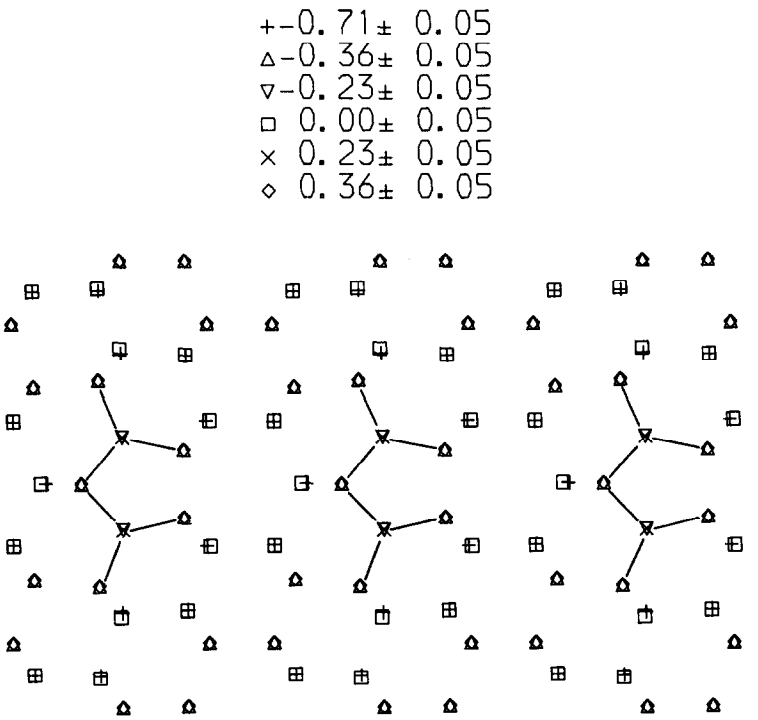

Fig. 9. Relaxed structure of $p2'mm'$ (1 × 2) symmetrical tilt boundary in Si. The boundary period has doubled along the projection direction. Atoms denoted by 'V' and 'X' have pinched together along the projection direction and bonded. The straight lines drawn in this figure, and Figs 10 and 11, represent the bonds between the atoms which have pinched together along the projection direction and their neighbours. The key gives the distance of the atoms above the plane of projection in units of the lattice parameter. Atoms within ±0.05 of these positions are represented by the same symbol.

way all atoms at the boundary are tetracoordinated. The relaxed structure shown in Fig. 9 is indistingishable from that shown in [11], which was obtained with a valence force field. In our calculation 56 atoms were relaxed using 4 recusion levels to a maximum force of 0.008 eV/Å. The maximum bond length distortion was 5.6% and deviations from the ideal bond angle varied between −16 and +21%. As before the dominant changes in the covalent bond energies are associated with the most stretched bonds and the spσ and ppσ contributions are the most affected. (We cannot show all the data for reasons of space.) Most of the Δ_i's are positive as before and the three that are nagative belong to the only three atoms which have negative on-site energy changes. The LDOS's show no deep states and are almost identical to that of the perfect crystal from one lattice parameter either side of the boundary and beyond.

It is seen from Table 3 that the *pm* (1 × 2) and *cm* (2 × 2) structures of [15, 10] have the lowest energy, although we are not able to discriminate between them with the accuracy at 8 levels. The structures are shown in Figs 10 and 11. It is seen that all atoms are four-fold coordinated. They both combine the reconstruction along [1$\bar{1}$0] proposed in [11] with the experimentally observed translation state although only the *cm* structure has the correct plane symmetry. 140 atoms were relaxed for the *pm* structure using 6 recursion levels to a maximum force of 0.004 eV/Å. In the *pm* structure the bond length variations are between −2.5 and +5.9% and the bond angle variations are between −17 and +15%, 328 atoms were relaxed for the *cm* structure using 6 recursion levels to a maximum force of 0.005 eV/Å. This corresponds to 20 layers being relaxed on either side of the boundary. In the *cm* structure the bond length variations are between −2.2 and +5.2% and the bond angle variations are between −16.6 +14.3%. Although these distortion limits are very slightly less than they are in the *pm* structure it is not at all clear from inspection of the covalent bond energies and site energies why the *cm* structure should be slightly lower in energy. The experimental observation [80] that the *cm* structure is always seen at room temperature and the *pm* structure has never been seen indicates that the *cm* structure at room temperature is considerably more stable than our 0 K calculation would suggest. In both structures most of the Δ_i's are positive and the s–p mixing changes by less than 3%. The LDOS's of both structures show no states inside the band gap.

7. (1$\bar{3}$0) SYMMETRICAL TILT BOUNDARY IN SILICON

7.1. Review of experimental observations

This boundary has been studied by electron diffraction by Bacmann *et al.* [81] who established

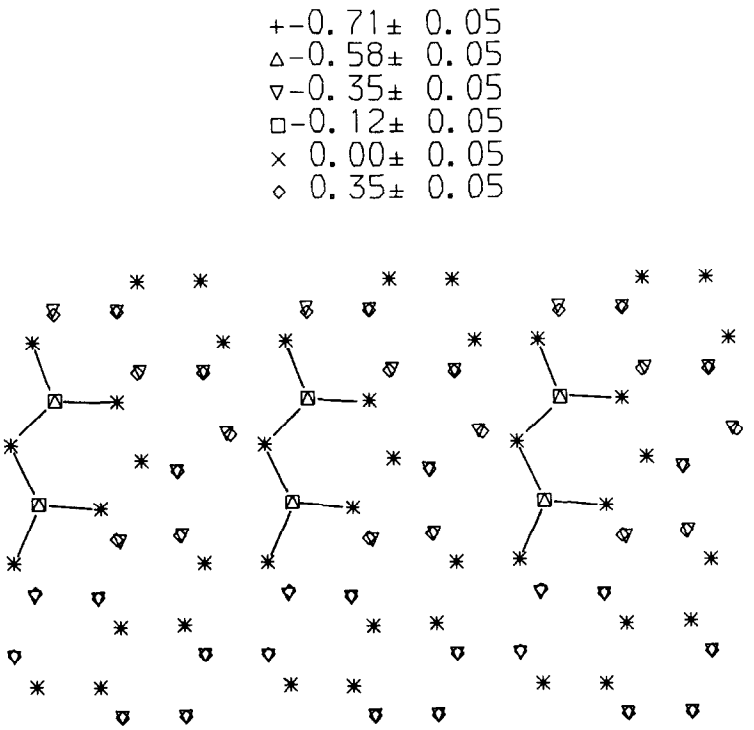

Fig. 10. Relaxed structure of *pm* (1 × 2) (11$\bar{2}$) symmetrical tilt boundary in Si. The boundary period has doubled along the period direction. Atoms represented by '□' and Δ have pinched together along the projection direction and bonded.

that the Shubnikov group is $p2_1'$. The translation state was also determined approximately in [81] by the α-fringe method as $\frac{1}{81}$[001] along the tilt axis and an expansion of 0.0075[1$\bar{3}$0]. Using this information they constructed a model of the boundary in which all atoms are tetracoordinated. Bonnet [82] obtained 3/20[001] for the translation along the tilt axis using the simultaneous two beam matching method of [83]

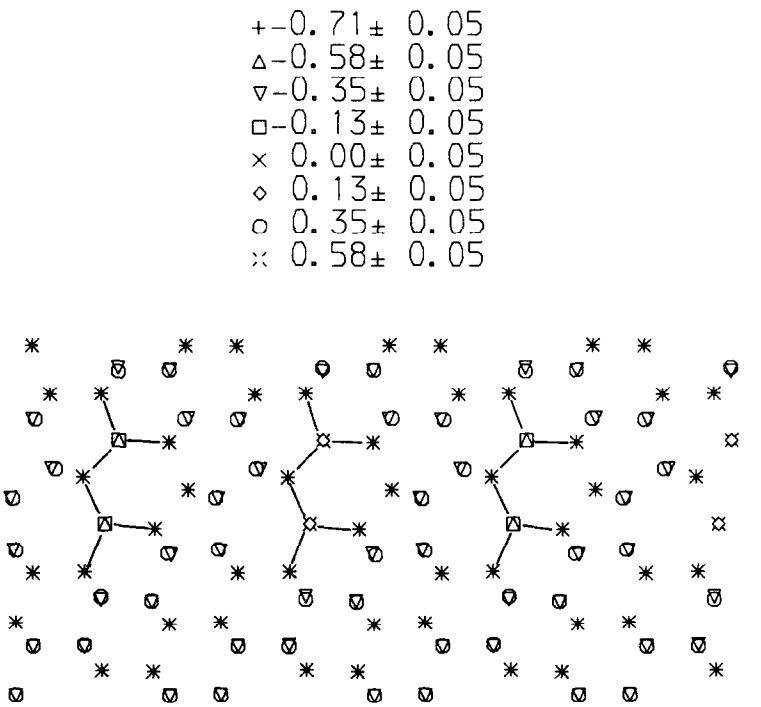

Fig. 11. Relaxed structure of *cm* (2 × 2) (11$\bar{2}$) symmetrical tilt boundary in Si. The boundary period has doubled both along the projection direction and along the horizontal direction. Atoms represented by '□' and 'Δ' have pinched together along the projection direction and bonded as have atoms represented by '⋇' and '◇'.

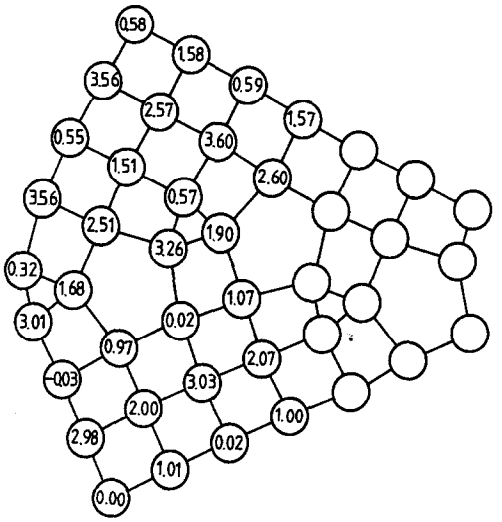

Fig. 12. Relaxed structure of $p2_1'$ (1 × 1) (1$\bar{3}$0) symmetrical tilt boundary in Si. Atoms are labelled with their distances above the (001) projection plane in units of $\frac{1}{4}$[001] for comparison with Fig. 7(b) of [81].

for a Δt dislocation separating two domains with opposite translation states.

7.2. *Results*

We have relaxed the model of Bacmann *et al.* to 6 recursion levels and a maximum force of 0.006 eV/Å. We find that the structure is stable even though the $2_1'$ axis symmetry could be broken during the relaxation and we obtained a translation vector of 0.144[001] along the tilt axis and an expansion of 0.01[1$\bar{3}$0]. Our translation along the tilt axis is within experimental error of Bonnet's measurement of 0.150[001]. Figure 12 shows the relaxed structure of the boundary in a way which makes it readily compared with Fig. 7(b) of [81].

We find a remarkably low grain boundary energy of $300 \pm 10\,\mathrm{mJ/m^2}$. The sp-mixing changes by less than 2% and most of the Δ_i's are positive. The bond length changes vary between −2.4 and 4.4% and the bond angle distortions vary between 13 and 14%. The LDOS's show no states inside the band gap.

8. DISCUSSION

8.1. *The model and its solution*

Unlike classical inter-atomic potentials, the tight-binding method has the advantage that it leaves room for many improvements as its limitations become evident. This is because it has a sound basis in quantum theory; and any approximation made, either in constructing the Hamiltonian or in solving Schrödinger's equation, can be recovered at the expense of greater complexity. We have presented an internally consistent, real space solution of the electronic and atomic structures of planar defects in Si. That is, the interdependence of the atomic and electronic structures is treated *explicitly*, with an approximate form of self-consistency in the form of local charge neutrality. The solution of the Schrödinger equation in real space, via the recursion method, allows one to consider defects lacking translational symmetry. Moreover there exists in principle a certain number of atoms above which the recursion method becomes a faster solution of the Schrödinger equation than a straight diagonalization of the Hamiltonian with a supercell geometry in **k** space. We estimate that in Si with only four-fold coordination and a minimal basis set this number is between 100 and 200 atoms.

Clearly a number of approximations and assumptions have been made to arrive at a tractable scheme for large scale defect calculations. A large number of these approximations and assumptions are removed if all the integrals involved in determining Hamiltonian and overlap matrix elements are calculated using an explicit atomic-orbital-like basis and ionic or chemical pseudopotentials [84]. In this way the bond integrals themselves become dependent on the atomic environment through crystal field terms. One can obtain the charge density $\rho(r)$ from the density matrix and the basis and iterate to self-consistency if required with the local density approximation, e.g. [85].

There is a problem associated with the use of equation (2.6) to calculate interatomic forces that arise from the inexactness of the density matrix elements in equations (2.5 and 2.6). Equation (2.6) is correct provided the density matrix elements are exact. The inexactness of the matrix elements leads to a further contribution to the derivative of the binding energy which is proportional to the derivative of the error in the density matrix elements. The error in the density matrix elements leads to an inconsistency between the numerical derivative of equation (2.4) and the analytic derivative in equation (2.6). We have carried out numerical tests to establish the variation of the error in equation (2.6) with the number of recursion levels using a square root terminator, and requiring local charge neutrality. For Chadi's Hamiltonian we find that the numerical and analytic derivatives differ by less than 10% when the number of levels is $\geqslant 2$ and that it diminishes relatively slowly and non-uniformly with number of levels.

8.2. *The form of the pair potential*

We have examined the properties of pair potentials of both inverse fourth and fifth power form. The inverse fourth power is based on Harrison's assumption that the repulsive energy is dominated by overlap between valence orbitals, and that the overlap integrals scale as the inverse square. However the valence overlap in Si scales more like the inverse of the interatomic distance so that valence orbital overlap should give a pair potential scaling like inverse cube [42]. Furthermore, it has also been argued that the tight-binding repulsive energy is rather the result of non-orthogonality between valence orbitals on one site and core wavefunctions on the other [42, 86]. In

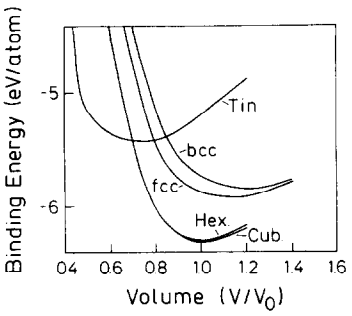

Fig. 13. Binding energy–volume curves as in Fig. 1 (a) except that a $1/r^5$ repulsive pair potential has been used instead of $1/r^4$ in Fig. 1 (a).

both contributions are taken into account, van Schilfgaarde [88] finds a repulsive energy which is a sum of terms in $1/r^3$ and $1/r^8$ for which Majewski and Vogl's [89] $1/r^5$ energy is a reasonable compromise (although they assumed an inverse cube scaling of the overlap between valence orbitals to arrive at the inverse fifth power). We show in Fig. 13 energy–volume curves using the inverse fifth power repulsive energy; and in Table 8, the cohesive energy and bulk modulus (the latter from a 15-recursion level calculation).

The zero of binding energy in Figs 4 and 13 is the energy of atoms of paramagnetic Si infinitely separated *in vacuo*. To make comparison with experiment, it is necessary to include the energy difference between these hypothetical atoms and gaseous Si atoms which have a magnetic moment due to the two p-electrons having the same spin direction by Hund's rule. The spin-polarisation energy in Si is 0.757 eV/atom [91] and this should be added to our plotted binding energies when making comparison with experimental values† (this correction was included in Yin and Cohen's calculations [58] shown in Fig. 4 although their cohesive energy was not in agreement with more recent results shown in Table 8). The spin polarisation correction is simply a matter of changing the zero of energy in our calculations, so we have not included it in Figs 4 or 13 which show binding energies obtained from equation (2.4); but we include it in Table 8 in order to evaluate the properties of the two pair potentials.

Comparing the bulk modulus with experiment and the cohesive energy with an accurate quantum mechanical calculation, we see that the inverse fifth power repulsive potential gives a better description that the inverse fourth. Also the equilibrium volumes of the close packed structures are better reproduced, but the minimum energy of the beta-tin structure is incorrectly higher than that of the close-packed structures. We discovered these results after completing our calculations on the grain boundaries with the inverse fourth power potential. In future calculations we would recommend the use of the inverse fifth power potential.

†We are grateful to R. Jones for pointing out this omission in our earlier paper [6].

Table 8. Cohesive energy (corrected for spin polarisation) and bulk modulus for inverse fourth and inverse fifth power repulsive energies

	Cohesive energy (eV/atom)	Bulk modulus (Mbar)
Inverse fourth	3.94	0.46
Inverse fifth	5.57	0.75
Density functional result	5.28 [90]	0.94 [90]
Experiment [97]	4.70	0.99

8.3. Results for grain boundaries in Si

8.3.1. Atomic structures. The grain boundaries selected in this study have been the subject of detailed experimental investigations. For both the $(11\bar{2})$ and $(1\bar{3}0)$ boundaries we have found that stable structures exist with translation states within experimental error of those measured. In the case of the $(11\bar{2})$ boundary we found that the lowest energy structure, among the five reconstructions proposed by other authors, is indeed the structure which has been proposed in [10] on the basis of high resolution electron microscopy and electron diffraction observations. However the energy of this structure in our work comes out too close to the energy of the closely related *pm* (1×2) structure [15] for our calculation to distinguish convincingly between them.

Kohyama *et al.* have used Chadi's **k**-space method to study the $(1\bar{3}0)$ and *cm* $(11\bar{2})$ [21] symmetrical tilt boundaries in Si. Although the tight-binding Hamiltonian is identical to that used in this work their repulsive pair potential is also the same as that used by Chadi [18] and is therefore different from that used here. Moreover there was no attempt at self-consistency in [21]. Despite this the relaxed atomic structures and boundary energies obtained by Kohyama *et al.* are virtually indistinguishable from those reported here. The reason why the atomic structures and energies appear to be insensitive to the pair potential must be the relatively small deviations of the bond lengths from the ideal value. The reason for the insensitivity to self-consistency is discussed in Section 8.3.4.

It is not possible to be sure that the structures we have obtained are the only metastable states for these boundaries or indeed to be certain that the global minima have been found. The configurational phase space associated with a grain boundary in Si appears to admit an unusual variety of metastable states because the diamond cubic structure is so open and because there is no reason to assume that the period of the boundary is necessarily the same as that of the coincidence site lattice. Our philosophy has been to seek guidance from experimental observations in sampling the configurational phase space. The alternative is to carry out a molecular dynamics or Monte Carlo simulation. In addition to the difficulties of smoothly terminating the $1/d^2$ scaling relation for the

Hamiltonian between first and second neighbour distances, such simulations would at present be prohibitively expensive. We note that this is also true for the Car–Parrinello simulations [24]. Clearly there is a need to develop reliable *classical* potentials for Si so that simulated annealing may be carried out inexpensively and accurately. However, on a cautionary note, recent work by Wilson and Sutton [92] on the structures of surfaces of Si indicates that the potentials of Stillinger and Weber [60] and Baskes [93] are unable to correctly predict the π-bonded chain model as the lowest energy structure for the (111) 2×1 surface in Si.

8.3.2. Electronic structures. The LDOS's indicate how the electronic structure in the boundary differs from that of the bulk. We can define a "LDOS width of the grain boundary" as twice the distance from the geometrical boundary plane at which the normalized overlap between the LDOS's and the LDOS in the perfect crystal exceeds some arbitrary high value such as 90%. In all our calculations this width is the same as the structural width of the boundary, inside which most of the bond angle and length distortions occur. This width is typically around 10 Å. It is also in this region that any significant rehybridisation occurs. Thus the boundary energy is dominated by a relatively narrow region about the geometrical boundary plane. However the relatively small relaxations in the more remote regions are crucial in that they allow and accommodate the large distortions in the narrow region.

In Section 4.2.3 we showed that the LDOS on an atom was dominated by the disposition of atoms comprising the first neighbour shell. This is an illustration of Friedel's local invariance theorem which has been discussed particularly clearly by Heine [34]. The significance of this result is that it suggests that the decomposition of a longer period boundary structure into structural units of shorter period boundaries is a good first approximation to the electronic structure of the longer period boundary. The largest errors in this approximation will correspond to atoms common to two different structural units. We have confirmed this conjecture by examining the LDOS's on atoms in the *pm* (1×2) and *cm* (2×2) $(11\bar{2})$ boundaries. The (2×2) boundary is composed of a succession of structural units of the (1×2) boundary displaced along the tilt axis.

In those boundaries which contain only four-fold coordinated atoms it was found that there were no states deep inside the band gap. Indeed the only boundary for which deep states were found was the (1×1) $p2'mm'$ $(11\bar{2})$ boundary which contained three-fold coordinated atoms. Our real-space solution of the Schrödinger equation to 40 recursion levels does not have sufficient resolution to determine whether there are band tails associated with the valence and conduction bands. However, Kohyama *et al.* [21] have studied the projected band structures of the relaxed *cm* $(11\bar{2})$ and $(1\bar{3}0)$ boundaries and found localised states at the edges of the valence and conduction bands. Similarly DiVincenzo *et al.* [23] found localised states at the edges of the valence and conduction bands in their study of the (221) symmetrical tilt boundary in Si. But in all cases these localised states are above the minimum of the conduction band or below the maximum of the valence band and therefore *they do not give rise to band tails in the density of states.* That is, these localised states are buried in the density of states under the valence and conduction band edges. These localised states are caused by the deviations of bond lengths and angles from their ideal tetrahedral values. In Refs [21, 23] these deviations give rise to only "off-diagonal disorder" in the Hamiltonian. In our work there is both off-diagonal and "diagonal disorder" in the Hamiltonian caused by the requirement of local charge neutrality. The variations in the Hamiltonian matrix elements are generally less than 0.5 eV in the boundaries. Not surprisingly the largest variations in the diagonal Hamiltonian matrix elements arise in boundaries containing atoms which are not four-fold coordinated.

These results appear to be in disagreement with experimental measurements of the densities of states in the band gap of bicrystals and polycrystals of Si [4]. These authors find a continuum of states in the middle of the band gap and exponential band tails extending into the gap from both the valence and conduction bands. These results were obtained for specimens grown both by the Czochralski method and the float-zone method. The latter should contain fewer impurities than the former.

Queisser and Werner [4] and Werner and Peisl [94] ascribe the origin of band tails to the intrinsic structural disorder within the boundary which causes short-range fluctuations in the potential leading to localization of the free carriers. These potential fluctuations are identical to the variations in the Hamiltonian matrix elements at the boundaries which we have just discussed. In the tight-binding models these fluctuations do indeed give rise to localised states in the band gap in the projected band structure but not to band tails in the density of states. Therefore the following question arises: is there some lower limit of structural disorder within the boundary which is necessary to produce a localised state below the conduction band minimum or above the valence band maximum? In a two-dimensional system any degree of disorder leads to some localisation, whereas in three dimensions there is a critical degree of disorder that must be exceeded before localisation sets in. This raises the possibly more fundamental question of whether there exists a critical degree of disorder that must be exceeded in the boundary plane to produce any localisation bearing in mind that the boundary is coupled electronically to two three-dimensional crystals. Similar questions can be asked about the existence of localised states at dislocations. It is likely that the boundaries that have been studied

experimentally contain steps, dislocations, facet junctions or curved segments. All of these intrinsic structural features are absent in the models, and may provide the necessary minimum distortions of bond lengths and angles to produce band tails. In our opinion it is more likely that the tails are caused by segregated impurities at the boundaries. However, Strunk and Werner [96] reported that they could not detect any impurities at the boundaries they studied in the electron microscope.

Our work indicates that midgap states are produced when three-fold coordinated atoms are present, but the high energy (1–2 eV) associated with these defects indicates that the fraction of three-fold coordinated sites present in the boundary in thermal equilibrium is vanishingly small up to the melting point of Si. Unless a mechanism of producing *and sustaining* a non-equilibrium distribution of these defects can be devised they can be discounted as the source of the experimentally observed [4] midgap continua. In our opinion the midgap states observed [4] with a density of 10^{10}–10^{12} states/eV/cm^2 are more likely to be caused by impurities.

8.4. Charge transfer and the importance of self-consistency

In this work we have required local charge neutrality as a form of self-consistency. This is in contrast to Chadi [18, 19] and Kohyama *et al.* [21], who did not attempt to achieve any form of self-consistency. In this section we discuss how significant the requirement of local charge neutrality is on the boundary energy and its atomic structure. We will show that provided the coordination is everywhere four-fold local charge neutrality has a negligible effect. But first we discuss the origin of charge transfer in the tight-binding model.

It was found in Sections 6 and 7 that, with four-fold coordination only, the Δ's were predominantly positive. This indicates that, in the absence of self-consistency, electronic charge tends to transfer to the boundary region form the adjoining grains. In the absence of self-consistency the diagonal Hamiltonian matrix elements do not change and therefore the first moment of the LDOS on each atom is equal to $\epsilon_s + 3\epsilon_p$. The zeroth moment is always equal to 8. Let N^i be the occupation of s and p orbitals at site i. The question then is how does N^i change when the second and higher moments of the LDOS on atom i change, but the zeroth and first moments remain fixed? Let us assume that N^i is determined by the second moment, μ_2^i, of the LDOS $n^i(E)$

$$\mu_2^i = \int_{-\infty}^{\infty} E^2 n^i(E)\, \mathrm{d}E = \sum_\alpha \mu_2^{i\alpha i\alpha}$$

where $n^i(E)$ is given by equation (4.1). The quantity we are interested in is

$$\left[\frac{\partial N^i}{\partial \mu_2^i}\right]_{\mu_0^i, \mu_1^i}.$$

To determine this derivative we have considered three model densities of states for the valence and conduction bands of Si: (i) two gaussians, (ii) two disjoint skew elliptic bands and (iii) two disjoint skew rectangular bands. We evaluated the above derivatives for the perfect crystal LDOS in which there is equal weight associated with each band. In all three cases the same result was obtained: *the above partial derivative is negative provided the width of the valence band is greater than the width of the conduction band.* Otherwise the partial derivative is zero or positive. Thus, there is a shift in weight from the conduction band to the valence bnad when μ_2^i is reduced. For Chadi's Hamiltonian the width of the valence band is approximately double the width of the conduction band. Therefore when μ_2^i is reduced N^i is increased and Δ_i must be positive in order to restore local charge neutrality. For a fixed μ_1^i, μ_2^i is determined by the sum of the squares of the hopping integrals from atom i to its neighbours. This sum is a complicated function of the angular disposition of the neighbours but it is always reduced if atom i is tetrahedrally coordinated and at a centre of dilatation. It is found that the majority of the second moments are reduced at the boundaries we have studied, as seen by the skewing of the valence band LDOS to higher energies and the conduction band LDOS to lower energies.

It is stressed that our simple analysis of the charge transfer is valid only for tight-binding Hamiltonians with wider valence bands than conduction bands. Moreover, our result applies only to the perfect crystal and small distortions from it; the derivative can change sign when it is evaluated at large distortions form the perfect crystal LDOS. Nevertheless the result reveals the importance of an accurate description of both the valence and conduction bands in determining charge transfer within the model. In reality the conduction band contains many plane wave states and the direction of the charge transfer may be reversed compared with our tight-binding model!

Suppose local charge neutrality has been achieved for some atomic assembly. How much does the binding energy of the assembly change if all the self-consistent changes in the diagonal Hamiltonian matrix elements are reset to zero? That is we switch off the self-consistency so that the model becomes the same as that used by Chadi and Kohyama *et al.* Since atoms are not moved the first order change in the binding energy is given by

$$\delta E_B^{(1)} = \mathrm{Tr}(\rho - \rho^f)\delta H$$

where δH is diagonal with elements $\delta H_{i\alpha i\alpha} = -\Delta_i$, and ρ is the density matrix for the assembly with local charge neutrality and ρ^f is the density matrix for a superposition of atomic charge densities (see section 2.3). It follows immediately that $\delta E_B^{(1)}$ is zero because of the local charge neutrality condition. Only diagonal terms contribute to the trace in $\delta E_B^{(1)}$. That is not to say, however, that the covalent bond energies do

not change to first order; rather their change is cancelled by a term arising from the change in the occupations of the orbitals which is part of the first order change in the site energy. Thus, to first order, the effect of switching off the local charge neutrality condition is simply to redistribute the binding energy among the covalent bond and site energies. There is a change in the binding energy to second order involving long range contributions from response functions [8]. This contribution is small provided the Δ's are small as in the presence of four-fold coordination. We have confirmed this numerically and found that the boundary energies change by about 10% when the local charge neutrality condition is switched off and there is four-fold coordination.

The atomic structure of the boundary is also influenced by the local charge neutrality condition. This is because the intersite density matrix elements, or partial bond orders, are affected by diagonal Hamiltonian matrix elements. The atomic structure of the boundary (at 0K) is determined by the interatomic forces. Therefore we consider now how the force on an atom changes when local charge neutrality has been achieved and a single Δ_j is switched off. The contribution to the force on atom i in the x direction which is affected by changes in the tight-binding Hamiltonian is given by

$$f_i^x = -\mathrm{Tr}(\rho - \rho^{\mathrm{f}})\frac{\partial H}{\partial X_i}.$$

The first order change in this force when Δ_j is set to zero is given by

$$\begin{aligned}\delta f_i^x &= -\Delta_j \frac{\partial f_i^x}{\partial \Delta_j} \\ &= -\Delta_j \frac{\partial}{\partial \Delta_j}\frac{\partial}{\partial x_i}\mathrm{Tr}(\rho - \rho^{\mathrm{f}})H \\ &= -\Delta_j \frac{\partial N_j}{\partial x_i}.\end{aligned}$$

The last equality follows by reversing the order of differentiation. (It will be recalled that the elements of ρ^{f} are constant.) Since μ_0^j and μ_1^j are unaffected by a virtual displacement of atom i we can write

$$\frac{\partial N_j}{\partial x_i} = \sum_{r=2}^{\infty}\frac{\partial N_j}{\partial \mu_r^j}\frac{\partial \mu_r^j}{\partial x_i}.$$

The local invariance theorem [34] tells us that the dominant contributions arise when i and j refer to the same atom or when they are nearest neighbours of each other. Thus we can approximate the infinite sum very well by its first term

$$\frac{\partial N_j}{\partial x_i} \simeq \frac{\partial N_j}{\partial \mu_2^j}\frac{\partial \mu_2^j}{\partial x_i}.$$

If all the Δ's are switched off the change in the force on any particular atom, i, has contributions from each of its neighbours, j, proportional to $(\Delta_j \partial N_j/\partial \mu_2^j + \Delta_i \partial N_i/\partial \mu_2^i)$. This is unlikely to be a significant contribution if the Δ's are small, as they are when the coordination is four-fold. These insights into the magnitude and range of δf_x^i have been confirmed numerically.

Acknowledgements—We have benefited from correspondence with M. Kohyama and J. Werner. M. Kohyama kindly sent us preprints of his recent publications. A.T.P. is grateful to the SERC for a studentship and, more recently, to the Max-Planck Gesellschaft and SERC for financial support. A.P.S. gratefully acknowledges the continuing support of the Royal Society and Professor Sir Peter Hirsch F.R.S. for encouragement and laboratory facilities. The calculations were performed on the SERC Cray-XMP at Rutherford Laboratory.

REFERENCES

1. C. R. M. Grovenor, *J. Phys. C, Solid St. Phys.* **18,** 4079 (1985).
2. *Polycrystalline Semiconductors*, Springer series in solid state sciences, **57,** (edited by G. Harbeke), Vol. 57. Springer, Berlin (1985).
3. J.-L. Maurice, *Revue Phys. Appl.* **22,** 613 (1987).
4. H. J. Queisser and J. Werner, *Mater. Res. Soc. Symp. Proc.* **106,** 53 (1988).
5. *Colloque International sur les Semiconducteurs Polycristallins, J. Physique* **43,** C-1 (1982).
6. A. T. Paxton, A. P. Sutton and C. M. M. Nex, *J. Phys. C, Solid St. Phys.* **20,** L263 (1987).
7. A. T. Paxton and A. P. Sutton, *J. Phys. C, Solid St. Phys.* **21,** L481 (1988).
8. A. P. Sutton, M. W. Finnis, D. G. Pettifor and Y. Ohta, *J. Phys. C, Solid St. Phys.* **21,** 35 (1988).
9. H. J. Möller and H. H. Singer, in Ref. [2], p. 18.
10. A. Bourret, L. Billard and M. Petit, *Microscopy of Semiconducting Materials*, Inst. Phys. Conf. Ser. No. 76, p. 23 (1985).
11. R. C. Pond, D. J. Bacon and A. M. Bastaweesy, *Microscopy of Semiconducting Materials*, Inst. Phys. Conf. Ser. No. 76, p. 253 (1985).
12. J. T. Wetzel, A. A. Levi and D. A. Smith, *Mater. Res. Soc. Symp. proc.* **63,** 157 (1986).
13. S. Phillpot and D. Wolf, *Mater. Res. Soc. Symp. Proc.* **122,** 103 (1988).
14. J. Hornstra, *Physica* **25,** 409 (1959); **26,** 198 (1960); J. A. Kohn, *Am. Minerlgst* **43,** 263 (1958).
15. A. M. Papon and M. Petit, *Scripta metall.* **19,** 391 (1985).
16. W. A. Harrison, *Electronic Structure*. Freeman, San Francisco, Calif. (1980).
17. M. Kohyama, R. Yamamoto and M. Doyama, *Physica status solidi* (b) **136,** 31 (1986); *ibid* **137,** 11 (1986); *ibid* **138,** 387 (1986).
18. R. E. Thomson and D. J. Chadi, *Phys. Rev. B* **29,** 889 (1984).
19. (a) D. J. Chadi, *Phys. Revt.* **41,** 1062 (1978); (b) D. J. Chadi, *Phys. Rev. B* **19,** 2074 (1984); (c) D. J. Chadi, *Phys. Rev. B* **29,** 785 (1984); (d) Q. Gou-Xin and D. J. Chadi, *Phys. Rev. B* **35,** 1288 (1987).
20. V. Heine, R. Haydock, D. W. Bullett and M. J. Kelly, *Solid St. Phys.*, Vol. 35 (1980).
21. M. Kohyama, R. Yamamoto, Y. Ebata and M. Kinoshita, *J. Phys. C, Solid St. Phys.* **21,** 3205 (1988); M. Kohyama, R. Yamamoto, Y. Watanabe, Y. Ebata and M. Kinoshita, *J. Phys. C, Solid St. Phys.* **21,** L695 (1988).
22. A. Bourret and J. J. Bacmann, *Surf. Sci.* **162,** 495 (1985).
23. D. P. DiVincenzo, O. L. Alerhand, M. Schlüter and J. W. Wilkins, *Phys. Rev. Lett.* **56,** 1925 (1986).

24. M. C. Payne, P. D. Bristowe and J. D. Joannopoulos, *Phys. Rev. Lett.* **58,** 1348 (1987).
25. M. C. Payne, J. D. Joannopoulos, D. C. Allan, M. P. Teter and D. H. Vanderbilt, *Phys. Rev. Lett.* **56,** 2656 (1986).
26. R. Car and M. Parrinello, *Phys. Rev. Lett.* **55,** 2471 (1985).
27. C. A. Coulson, *Proc. R. Soc. A* **169,** 413 (1939); *Valence.* Clarendon Press, Oxford (1952).
28. J. C. Slater and G. F. Koster, *Phys. Rev.* **94,** 1498 (1954).
29. D. J. Chadi and M. L. Cohen, *Physica status solid* (b) **68,** 405 (1975).
30. P. A. M. Dirac, *The Principles of Quantum Mechanics.* Clarendon Press, Oxford (1930).
31. L. I. Schiff, *Quantum Mechanics.* McGraw-Hill, New York (1955).
32. A. R. Williams, P. J. Feibelman and N. D. Lang, *Phys. Rev. B* **26,** 5433 (1982).
33. D. G. Pettifor, in *Physical Metallurgy* (edited by R. W. Cahn and P. Haasen), Chap. 3. North-Holland, Amsterdam (1983).
34. V. Heine, in Ref. [20].
35. W. Kohn and L. J. Sham, *Phys. Rev.* **140,** A113 (1965).
36. J. Harris, *Phys. Rev. B* **31,** 1770 (1985).
37. C. Priester, G. Allan and M. Lannoo, *Phys. Rev. B* **33,** 7386 (1986).
38. Y. Ohta and M. W. Finnis, unpublished research.
39. B. Legrand, *Phil. Mag. A* **52,** 83 (1985).
40. V. Heine, *Phys. Rev.* **145,** 593 (1966).
41. K. S. Singwi and M. P. Tosi, *Phys. Rev.* **181,** 784 (1969).
42. M. van Shilfgaarde and A. Sher, *Phys. Rev. B* **36,** 4375 (1987).
43. W. A. Harrison, *Phys. Rev. B* **27,** 3592 (1983).
44. R. Haydock, in Ref. [20].
45. A. Mauger, J. C. Bourgouin, G. Allan, M. Lannoo, A. Bourret and L. Billard, *Phys. Rev. B* **35,** 1267 (1986).
46. M. Hashimoto, Y. Ishida, R. Yamamoto and M. Doyama, *Acta metall.* **32,** 1 (1984); M. Hashimoto, Y. Ishida, S. Wakayama, R. Yamamoto, M. Doyama and T. Fujiwara, *Acta metall.* **32,** 13 (1984).
47. C. M. M. Nex, *J. Phys. A* **11,** 653 (1978).
48. F. Ducastelle and F. Cyrot-Lackmann, *J. Phys. Chem. Solids* **31,** 1295 (1970).
49. T. J. Stieltjes, *Ann. Fac. Sci. Toulouse* **8,** A.1 (1895); *Oeuvres Completes*, Vol. II, p. 469. Noordhoff, Groningen (1918).
50. M. Mostoller and T. Kaplan, *Phys. Rev. B* **19,** 552 (1979).
51. R. Jones and M. W. Lewis, *Phil. Mag. B* **49,** 95 (1984).
52. J. Inoue and Y. Ohta, *J. Phys. C, Solid St. Phys.* **20,** 1947 (1987).
53. A. T. Paxton, *Phil. Mag. B.* **58,** 603 (1988).
54. C. M. M. Nex, M.Sc. thesis, Univ. of Sussex (1967).
55. S. Glanville, A. T. Paxton and M. W. Finnis, *J. Phys. F, Metal Phys.* 8, 693 (1988).
56. D. J. Chadi and R. M. Martin, *Sol. St. Commun.* **19,** 643 (1976).
57. D. C. Allan and E. J. Mele, *Phys. Rev. Lett.* **53,** 826 (1984); A. Mazur and J. Pollmann, *Phys. Rev. Lett.* **57,** 1811 (1986); M. Schmeits, A. Mazur and J. Pollmann, *Phys. Rev. B* **27,** 5012 (1983).
58. M. T. Yin and M. L. Cohen, *Phys. Rev. B* **26,** 5668 (1982).
59. K. C. Pandey and J. C. Phillips, *Phys. Rev. Lett.* **32,** 1433 (1974); *Phys. Rev. B* **13,** 750 (1976).
60. F. Stillinger and T. Weber, *Phys. Rev. B* **31,** 5262 (1985).
61. G. S. Painter, D. E. Ellis and A. R. Lubinski, *Phys. Rev. B* **4,** 3612 (1972).
62. V. G. Eremenko and V. I. Nikitenko, *Physica status solidi* (a) **14,** 317 (1972).
63. C. M. M. Nex, *Comp. Phys. Commun.* **34,** 101 (1984).
64. T. Y. Tan, H. Foll and S. M. Hu, *Phil. Mag. A* **44,** 127 (1981).
65. K. J. Chang and M. L. Cohen, *Phys. Rev. B* **31,** 7819 (1985).
66. V. Vitek, *Scripta metall.* **9,** 611 (1975).
67. S. G. Louie, *J. Physique* **46,** C4-335 (1985).
68. D. M. Duffy and P. W. Tasker, *J. Physique* **46,** C4-185 and refs therein (1985).
69. D. M. Greig, *Optimisation*, p. 56. Longman, London (1980).
70. D. Wolf, *Acta metall.* **32,** 245 (1984).
71. A. Bourret and J. J. Bacmann, *proc. JIMIS-4, Trans. Japan Inst. Metals*, Suppl. 125 (1986).
72. M. Prutton, *Surface Physics*, Clarendon Press, Oxford (1983).
73. A. Rocher and M. Labidi, *Rev. Phys. Appl.* **21,** 201 (1986).
74. C. Fontaine and D. A Smith, *Appl. Phys. Lett.* **40,** 153 (1982); D. Vlachavas and R. C. Pond, *Inst. Phys. Ser. Conf.* No. 60, 159 (1981).
75. R. C. Pond, private communication.
76. S. Marklund, *Physica status solidi* (b) **92,** 83 (1979).
77. R. C. Pond and D. Vlachavas, *Proc. R. Soc. A* **386,** 95 (1983).
78. H. J. Möller, *Phil. Mag. A* **43,** 1053 (1981).
79. R. C. Pond, *J. Physique* **43,** C1-51 (1982).
80. A. Bourret, private communication.
81. J. J. Bacmann, A. M. Papon, M. Petit and G. Silvestre, *Phil. Mag. A* **51,** 697 (1985).
82. R. Bonnet, *J. Physique* **46,** C4-61 (1985).
83. C. T. Forwood and L. M. Clarebrough. *Acta metall.* **30,** 1443 (1982).
84. W. M. C. Foulkes, Ph.D. thesis, Univ. of Cambridge (1987).
85. J. R. Chelikowsky and S. G. Louie, *Phys. Rev. B* **29,** 3470 (1984).
86. J. Friedel, *J. Physique* **39,** 651, 671 (1978).
87. D. G. Pettifor, *Solid St. Phys.* **40,** 43 (1987).
88. M. van Schilfgaarde, private communication.
89. J. A. Majewski and P. Vogl, *Phys. Rev. Lett.* **57,** 1366 (1986).
90. M. S. Hybertson and S. G. Louie, *Phys. Rev. B* **30,** 5777 (1984).
91. M. S. Methfessel, private communication.
92. J. H. Wilson and A. P. Sutton. To be published.
93. M. I. Baskes, *Phys. Rev. Letts* **59,** 2666 (1987).
94. J. Werner and M. Peisl, *Mater. Res. Soc. Symp. Proc.* **46,** 575 (1985).
95. J. Werner, private communication.
96. J. Werner and H. Strunk, *J. Physique* **43,** C1-89 (1982).
97. C. Kittel, *Introduction to Solid State Physics*, 4th edn. Wiley, New York (1971).